nature immunology

ARTICLES

https://doi.org/10.1038/s41590-019-0494-y

CD103^{hi} T_{reg} cells constrain lung fibrosis induced by CD103^{lo} tissue-resident pathogenic CD4 T cells

Tomomi Ichikawa[1,2,12], Kiyoshi Hirahara[1,3,12], Kota Kokubo[1,12], Masahiro Kiuchi[1], Ami Aoki[1], Yuki Morimoto[1], Jin Kumagai[1], Atsushi Onodera[1,4], Naoko Mato[5], Damon J. Tumes[1,6], Yoshiyuki Goto[7,8], Koichi Hagiwara[5], Yutaka Inagaki[9], Tim Sparwasser[10], Kazuyuki Tobe[2] and Toshinori Nakayama[1,11]*

Tissue-resident memory T cells (T_{RM} cells) are crucial mediators of adaptive immunity in nonlymphoid tissues. However, the functional heterogeneity and pathogenic roles of CD4$^+$ T_{RM} cells that reside within chronic inflammatory lesions remain unknown. We found that CD69^{hi}CD103^{lo} CD4$^+$ T_{RM} cells produced effector cytokines and promoted the inflammation and fibrotic responses induced by chronic exposure to *Aspergillus fumigatus*. Simultaneously, immunosuppressive CD69^{hi}CD103^{hi}Foxp3$^+$ CD4$^+$ regulatory T cells were induced and constrained the ability of pathogenic CD103^{lo} T_{RM} cells to cause fibrosis. Thus, lung tissue-resident CD4$^+$ T cells play crucial roles in the pathology of chronic lung inflammation, and CD103 expression defines pathogenic effector and immunosuppressive tissue-resident cell subpopulations in the inflamed lung.

Immunological memory is central to acquired immunity[1]. Memory T cells direct rapid and efficient protection against previously encountered pathogens[2]. Several subsets of memory T cell have been identified (that is, effector memory T cells (T_{EM} cells) and central memory T cells (T_{CM} cells))[3]. T_{EM} cells are abundant in nonlymphoid tissues and express low levels of the chemokine receptor CCR7 and CD62L, whereas T_{CM} cells express both CCR7 and CD62L[3]. Another subset of memory T cells—tissue-resident memory T cells (T_{RM} cells)—have been defined and are characterized by expression of the C-type lectin CD69 and the integrin CD103 (refs. [4–7]). T_{RM} cells preferentially localize in epithelial barrier tissues and are required for protection at mucosal sites, such as the respiratory tract, gastrointestinal tract, reproductive tract and skin, in both mice and humans[8–10].

Heterogeneity of effector T cell populations, including circulating memory T cells, has been well defined[11–14]. In the case of CD8$^+$ T_{RM} cells, distinct populations of CD8$^+$ T_{RM} cells play important roles in the pathology of T cell-mediated inflammatory diseases[15,16]. CD49a$^+$CD8$^+$ T_{RM} cells are enriched in the skin of patients with vitiligo, whereas interleukin-17 (IL-17)-producing CD49a$^-$CD8$^+$ T_{RM} cells are frequently detected in patients with psoriasis[15].

CD4$^+$ T cells in the lung aid the development of CD103^{hi}CD8$^+$ T_{RM} cells after influenza virus infection[17]. In a mouse model of vaginal herpes simplex virus infection, CD4$^+$ T_{RM} cells in the genital mucosa are required for full protection from herpes simplex virus[18]. Tissue regulatory T cells (T_{reg} cells) reside in nonlymphoid tissue and contribute to the maintenance of host homeostasis[19–21]. Pathogenic roles for memory CD4$^+$ T cells, which particularly memory-type pathogenic T_H2 cells that produce high levels of IL-5, have been identified[13,22]. Similar pathogenic T_H2 cells producing high levels of IL-5 have been reported in the skin of patients with atopic dermatitis[23], as well as the peripheral blood of patients with eosinophilic gastrointestinal and allergic diseases[24–26]. Amphiregulin-producing fibrosis-inducing pathogenic T_H2 cells have been identified in eosinophilic airway inflammation[27]. However, the functional heterogeneity and pathogenic roles of CD4$^+$ T_{RM} cells that reside within chronic inflammatory lesions remain unknown. Moreover, the molecular mechanisms through which CD4$^+$ T_{RM} cells are generated are largely undefined.

Fungi are the most widespread microbes encountered by mammalian hosts[28]. Sensitization to fungi plays a major role in the development, persistence and severity of lower airway diseases in patients with asthma[29]. Sensitivity to *Aspergillus fumigatus*, which is one of the most common environmental fungi, is associated with an increased risk of adult-onset asthma[30]. The underlying cellular and molecular mechanisms that control the chronic inflammation induced by fungal infection are poorly understood.

Herein, we investigate the function of CD4$^+$ T_{RM} cells involved in the pathogenesis of fibrotic responses during chronic lung inflammation induced by repeated exposure to *A. fumigatus*. We found that tissue-resident CD44^{hi}CD69^{hi} CD4$^+$ T cells had high expression of fibrosis-related genes, relative to circulating CD44^{lo} or CD44^{hi}CD69^{lo} CD4$^+$ T cells. Moreover, low expression of CD103 defined pathogenic effector CD4$^+$ T_{RM} cells, and high expression of CD103 defined tissue-resident immunosuppressive T_{reg} cells that possessed distinct transcriptional and epigenetic programs in the inflamed lung. Among CD44^{hi}CD69^{hi} CD4$^+$ T cells, CD103^{lo} CD4$^+$ T_{RM} cells promoted the pathology of fibrotic responses in the lung through the enhanced production of effector cytokines such as IL-5 and IL-13. In contrast, CD103^{hi} tissue-resident T_{reg} cells that

[1]Department of Immunology, Graduate School of Medicine, Chiba University, Chiba, Japan. [2]First Department of Internal Medicine, University of Toyama, Toyama, Japan. [3]AMED-PRIME, AMED, Chiba, Japan. [4]Institute for Global Prominent Research, Chiba University, Chiba, Japan. [5]Division of Pulmonary Medicine, Department of Medicine, Jichi Medical University, Shimotsuke, Japan. [6]Centre for Cancer Biology, University of South Australia and SA Pathology, Adelaide, South Australia, Australia. [7]Division of Molecular Immunology, Medical Mycology Research Center, Chiba University, Chiba, Japan. [8]Division of Mucosal Symbiosis, International Research and Development Center for Mucosal Vaccines, Institute of Medical Science, The University of Tokyo, Tokyo, Japan. [9]Center for Matrix Biology and Medicine, Graduate School of Medicine, Tokai University, Isehara, Japan. [10]Department of Medical Microbiology and Hygiene, University Medical Center, Johannes Gutenberg University Mainz, Mainz, Germany. [11]AMED-CREST, AMED, Chiba, Japan. [12]These authors contributed equally: Tomomi Ichikawa, Kiyoshi Hirahara, Kota Kokubo. *e-mail: tnakayama@faculty.chiba-u.jp

expressed Foxp3 ameliorated fibrotic responses. Thus, functionally distinct tissue-resident CD4+ T cell populations regulate the pathology of chronic inflammatory responses, including fungal-induced fibrotic responses in the lung.

Results

Repeated exposure to *Aspergillus* antigen resulted in chronic lung inflammation and lung fibrotic responses. Dysregulated inflammation promotes fibrotic changes in various organs, including the lung[31]. To investigate the immunological events that occur during fibrotic changes in the lung, we developed an experimental model in which mice were repeatedly exposed intranasally to *Aspergillus* antigen for 7 weeks (Supplementary Fig. 1a). A histological analysis of the lungs revealed massive infiltration of inflammatory cells around the bronchi (Fig. 1a). Repeated antigen exposure also induced fibrotic responses in the peri-bronchial region, as evidenced by increased staining by Sirius Red, as well as increased collagen levels in the lung compared with those in controls (Fig. 1b,c). The expression of the fibrotic signature gene collagen type 1 alpha 1 (*Col1a1*) was enhanced in the lungs of mice with repeated exposure to fungal antigen (Supplementary Fig. 1b). In addition, transgenic mice containing the enhancer and promoter sequences of the *Col1a2* gene linked to green fluorescent protein (collagen 1a2-GFP mice) showed increased GFP-positive cells that produced collagen in the lung (Supplementary Fig. 1c). Effector cytokines—particularly IL-5 and IL-13—were substantially increased in the bronchoalveolar lavage (BAL) fluid of mice repeatedly exposed to *Aspergillus* antigen (Supplementary Fig. 1d), and were associated with the infiltration of inflammatory cells, including eosinophils, neutrophils and lymphocytes, and enhanced airway hyper-responsiveness (Supplementary Fig. 1e,f). Thus, repeated exposure to *Aspergillus* antigen resulted in chronic lung inflammation accompanied by increased lung fibrotic responses.

Increased numbers of CD4+ T cells were detected in the lungs, but not the spleen, of *Aspergillus* antigen-exposed mice, and the lung CD4+ T cells had increased proportions of cells with a $CD44^{hi}CD62L^{lo}$ phenotype, suggesting that memory-type CD4+ T cells may be involved in the induction of fibrotic responses in this model of chronic lung inflammation (Supplementary Fig. 1g–i). Moreover, in T cell-deficient *Foxn1*^{nu} mice, the lung inflammation and fibrotic responses were significantly ameliorated, indicating that T cells play an important role in the lung pathology (Supplementary Fig. 1j,k).

Repeated exposure to *Aspergillus* antigen induced $CD69^{hi}$ CD4+ tissue-resident T cells in the inflamed lung. Repeated exposure to the fungus antigen induced a subpopulation of $CD44^{hi}CD62L^{lo}$ CD4+ T cells in the lungs that expressed high levels of CD69 (Fig. 1d). CD69 expression on $CD44^{hi}CD62L^{lo}$ CD4+ T cells in the spleen was unchanged by fungal exposure in the lungs (Supplementary Fig. 2a). To characterize the $CD44^{hi}CD62L^{lo}CD69^{hi}$ CD4+ T cells in the lungs, we performed an unbiased flow cytometry screening analysis. We identified 12 upregulated cell surface markers and one downregulated cell surface marker (Supplementary Fig. 2b). Among these molecules, CD103 (a ligand for E-cadherin) exhibited a bimodal expression pattern, while the other cell surface molecules did not (Fig. 1e and Supplementary Fig. 2c). $CD44^{hi}CD62L^{lo}CD69^{hi}$ CD4+ T cells from the inflamed lung, but not the spleen, exhibited increased numbers of $CD103^{hi}$ T cells compared with controls (Fig. 1f and Supplementary Fig. 2d–f). Since both CD69 and CD103 have recently been defined as markers for CD8+ tissue T_{RM} cells[5], we analyzed whether the $CD44^{hi}CD62L^{lo}CD69^{hi}$ CD4+ T cells were tissue resident. After repeated exposure to the *Aspergillus* antigen for 7 weeks, the mice were intravascularly injected with CD4-PE antibody and sacrificed 3 min later to distinguish between tissue-localized cells and blood-borne cells[32] (Supplementary Fig. 2g,h). Exposure to the fungal antigen induced substantial numbers of tissue-resident $CD44^{hi}$ CD4+ T cells in the inflamed lung (Supplementary Fig. 2i), but not the spleen (Supplementary Fig. 2j). In the control group, approximately 40% of the $CD44^{hi}CD69^{hi}$ CD4+ T cells were protected from in vivo labeling of by the CD4 antibody, and more than 95% were protected in the *Aspergillus* antigen-treated group (Fig. 1g,h and Supplementary Fig. 2k). In both the control and *Aspergillus* antigen-treated groups, the majority of $CD44^{lo}CD69^{lo}$ CD4+ T cells were circulating cells. Next, we analyzed the flow cytometry data using *t*-distributed stochastic linear embedding (*t*-SNE) plots—a dimensionality reduction method[33]. *t*-SNE plots confirmed that almost all of the $CD44^{hi}CD69^{hi}$ CD4+ T cells in the *Aspergillus* antigen-treated group were within the population protected from intravascular labeling of CD4 (Supplementary Fig. 2l). Consistent with these results, histological analysis of the inflamed lung exhibited massive infiltration of $CD69^{hi}$ CD4+ T cells, as well as collagen deposition (Fig. 1i,j and Supplementary Fig. 2m). Thus, repeated exposure to fungal antigen induced $CD69^{hi}$ CD4+ tissue-resident T cells in the inflamed lung.

Tissue-resident $CD69^{hi}$ CD4+ T cells expressed high levels of fibrosis-related genes. To determine the characteristics of CD4+ T cells induced by fungal antigen stimulation, we isolated four subpopulations of CD4+ T cells ($CD44^{lo}$, $CD44^{hi}CD69^{lo}$, $CD44^{hi}CD69^{hi}CD103^{lo}$ and $CD44^{hi}CD69^{hi}CD103^{hi}$ T cells) from the inflamed lung and examined the global gene expression profile by RNA sequencing (RNA-Seq; Fig. 2a and Supplementary Fig. 3a,b). Principal component analysis revealed that each subpopulation of CD4+ T cells exhibited a distinct transcriptional profile (Fig. 2a, bottom). In total, 27 and 56 genes were specifically expressed in $CD44^{hi}CD69^{hi}CD103^{lo}$ and $CD44^{hi}CD69^{hi}CD103^{hi}$ T cells, respectively (Supplementary Fig. 3c). Effector cytokines such as *Il17a*, *Ifng*, *Il4*, *Il13* and *Il5* were upregulated in $CD69^{hi}CD103^{lo}$ T cells but not in $CD69^{hi}CD103^{hi}$ T cells (Fig. 2b, left). The specifically upregulated genes in $CD69^{hi}CD103^{hi}$ T cells included *Foxp3*, *Klrg1*, *Prdm1* and *Rorc*, which indicated that $CD69^{hi}CD103^{hi}$ T cells express genes characteristic of T_{reg} cells[19,21,34] (Fig. 2b, right). *Pdcd1*, *Rora* and a series of chemokine receptors including *Cxcr6*, *Ccr4*, *Ccr2*, *Ccr5* and *Ccr8* were upregulated in both $CD69^{hi}CD103^{lo}$ and $CD69^{hi}CD103^{hi}$ T cells compared with $CD44^{lo}$ and $CD44^{hi}CD69^{lo}$ T cells (Supplementary Fig. 3d). Both $CD44^{hi}CD69^{hi}CD103^{lo}$ and $CD44^{hi}CD69^{hi}CD103^{hi}$ T cells expressed significantly less *S1pr1* than $CD44^{lo}$ and $CD44^{hi}CD69^{lo}$ T cells, and the low expression of *S1pr1* is required for the establishment of CD8+ T_{RM} cells[35] (Supplementary Fig. 3e,f). Both $CD69^{hi}CD103^{lo}$ and $CD69^{hi}CD103^{hi}$ T cells also exhibited downregulation of the chemokine receptor *Ccr7*, which is required for T cell exit from peripheral tissues[36] (Supplementary Fig. 3f). To validate the differential transcriptomes between $CD69^{hi}CD103^{lo}$ and $CD69^{hi}CD103^{hi}$ T cells, we performed a co-expression network analysis using $CD44^{lo}$, $CD69^{hi}CD103^{lo}$ and $CD69^{hi}CD103^{hi}$ T cells using a previously published method[37] (Fig. 2c). Overlaying the expression differences of the included genes revealed that one cluster was defined by $CD69^{hi}CD103^{lo}$ T cells, and the other was defined by $CD69^{hi}CD103^{hi}$ T cell-associated genes (Supplementary Fig. 3g). Fibrosis-related genes were upregulated in both tissue-resident $CD44^{hi}CD69^{hi}CD103^{lo}$ and $CD44^{hi}CD69^{hi}CD103^{hi}$ T cells compared with $CD44^{lo}$ or $CD44^{hi}CD69^{lo}$ T cells (Fig. 2d–f, Supplementary Fig. 3h and Supplementary Table 1) . Distinct sets of upregulated genes were observed in the $CD44^{hi}CD69^{hi}CD103^{lo}$ and $CD44^{hi}CD69^{hi}CD103^{hi}$ T cells. These results indicated that tissue-resident $CD69^{hi}$ CD4+ T cells were distinct in the transcriptome profile from circulating CD4+ T cells.

Tissue-resident $CD69^{hi}CD103^{lo}$ CD4+ T cells exhibit enhanced cytokine production. Approximately 12% of $CD69^{hi}CD103^{lo}$ T cells expressed GATA3 (the master regulator of T_H2 cells),

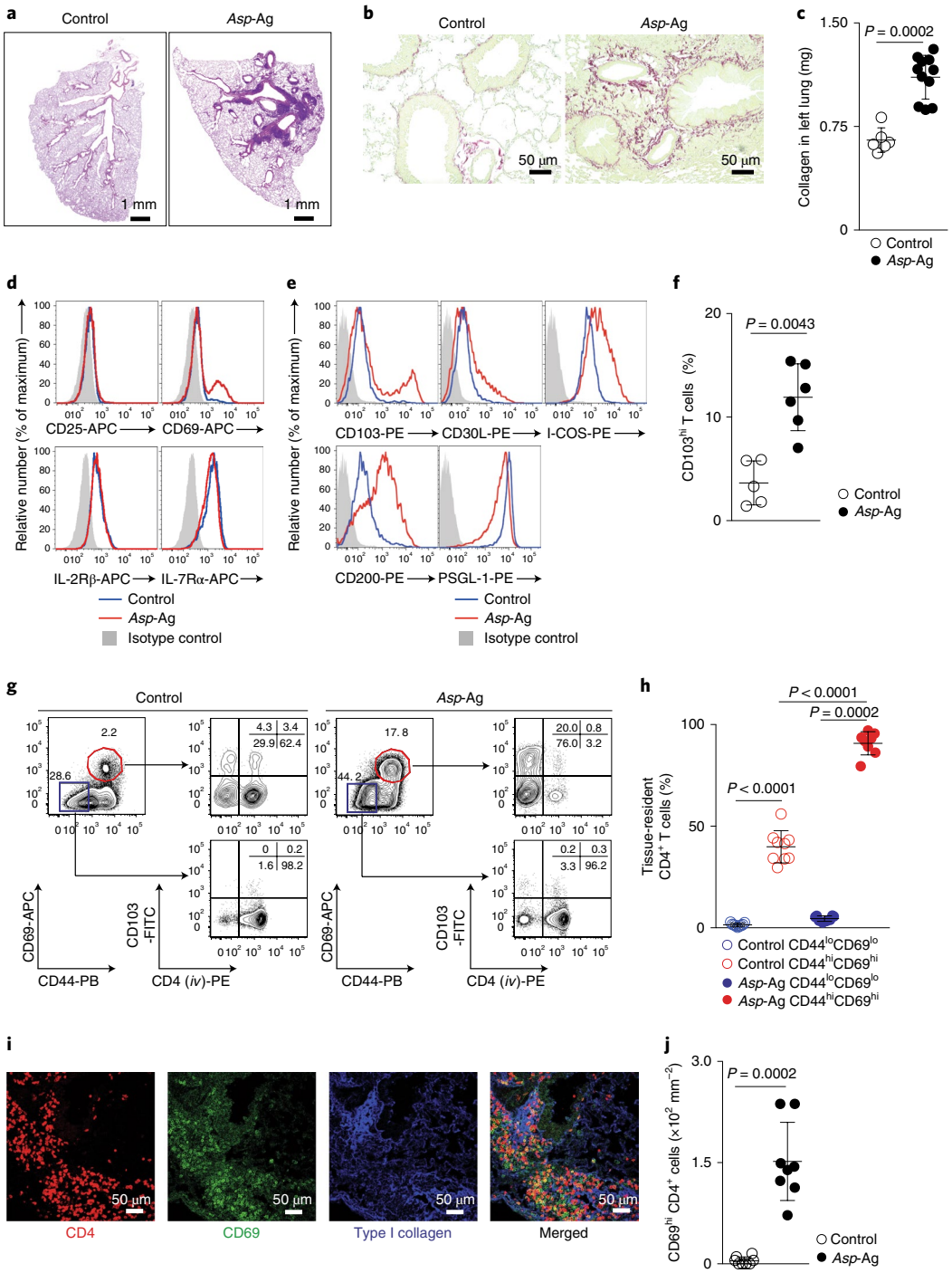

Fig. 1 | Repeated exposure to *Aspergillus* antigen induced tissue-resident CD4⁺ T cells in the inflamed lung. a, Representative histological sections of the lungs from control BALB/c mice (left) and *Aspergillus* antigen-exposed BALB/c mice (*Asp*-Ag; right). Sections were stained with hematoxylin and eosin. Ten mice per group were analyzed. **b**, Representative histological sections of the lungs from control and *Asp*-Ag mice. Sections were stained with Sirius Red. Ten mice per group were analyzed. **c**, Quantification of collagen protein in the lungs from control ($n=6$) and *Asp*-Ag mice ($n=11$). Pooled findings from two independent experiments are shown. **d**, Cell surface markers of CD44^{hi}CD62L^{lo} CD4$^+$ T cells in the lungs of control (blue lines) and *Asp*-Ag mice (red), along with the isotype-matched control antibody (gray). Representative findings from two independent experiments are shown. **e**, Cell surface markers on CD44^{hi}CD62L^{lo}CD69^{hi} CD4$^+$ T cells in the lungs of control (blue lines) and *Asp*-Ag mice (red), along with the isotype-matched control antibody (gray). **f**, Pooled data showing the proportion of CD103^{hi} T cells in CD44^{hi}CD62L^{lo}CD69^{hi} CD4$^+$ T cells from control ($n=5$) and *Asp*-Ag mice ($n=6$). Representative findings from two independent experiments are shown. **g**, Representative plots of intravenous staining of anti-CD4 and anti-CD103 staining in CD44^{hi}CD69^{hi} CD4$^+$ T cells (top) and CD44^{lo}CD69^{lo} CD4$^+$ T cells (bottom) in the lungs of control and *Asp*-Ag mice. iv, intravenous injection. **h**, Percentage of tissue-resident CD4$^+$ T cells in the CD44^{hi}CD69^{hi} CD4$^+$ T cell population (red) and CD44^{lo}CD69^{lo} CD4$^+$ T cell population (blue) from control (open symbols; $n=9$) and *Asp*-Ag mice (filled symbols; $n=8$). **i**, Representative confocal micrograph images of the lung stained with anti-CD4 (red), anti-CD69 (green) and anti-type I collagen (blue) from *Asp*-Ag mice. Representative findings of three independent experiments are shown. **j**, Absolute numbers of CD69^{hi}CD4$^+$ T cells in the lungs of control and *Asp*-Ag mice ($n=8$ mice per group). Data are presented as means ± s.d. in **c**, **f**, **h** and **j**. *P* values were calculated by two-sided Mann–Whitney *U*-test in **c**, **f**, **h** and **j**.

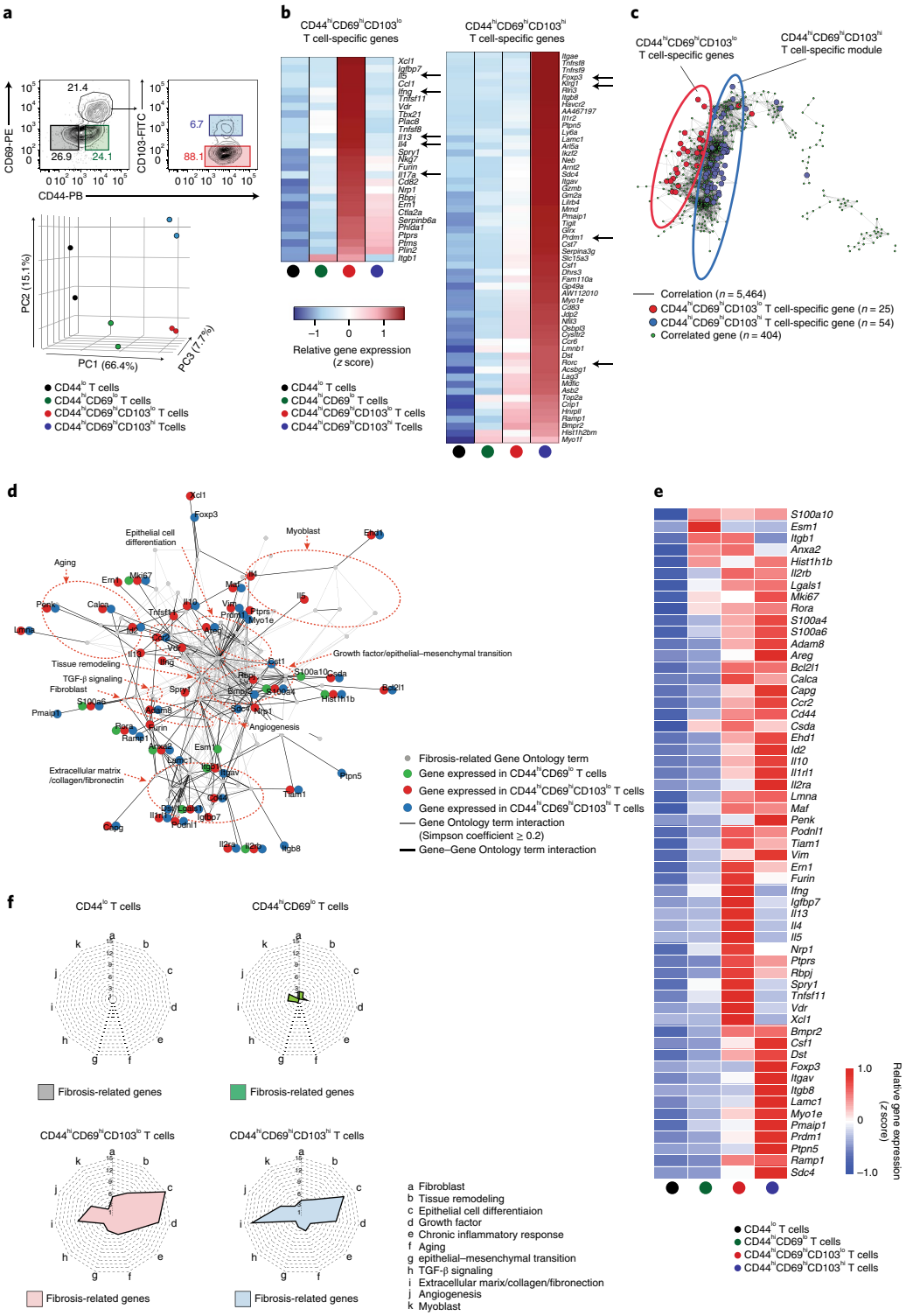

Fig. 2 | Tissue-resident CD69^{hi} T cells showed unique profibrotic features. a, Top: cell-sorting strategy for the four groups of CD4$^+$ T cells in the lungs of *Asp*-Ag mice. Bottom: principal component analysis plot of RNA-Seq data from four groups of CD4$^+$ T cells ($n = 8$). Duplicates of pooled samples are shown. **b**, Heat maps of genes with a greater than eightfold change in expression unique to CD44^{hi}CD69^{hi}CD103^{lo} (left; $n = 27$) or CD44^{hi}CD69^{hi}CD103^{hi} T cells (right; $n = 56$), compared with CD44^{lo} T cells, based on the mean value of each duplicate. **c**, Visualization of the co-regulation network based on the 487 genes selected using the criteria in the Methods. Red and blue nodes represent CD44^{hi}CD69^{hi}CD103^{lo} CD4$^+$ T cell-specific genes ($n = 25$) and CD44^{hi}CD69^{hi}CD103^{hi} CD4$^+$ T cell-specific genes ($n = 54$), respectively, as determined in Supplementary Fig. 2c. Red and blue ellipses reveal specific modules of CD44^{hi}CD69^{hi}CD103^{lo} and CD44^{hi}CD69^{hi}CD103^{hi} CD4$^+$ T cells, respectively. **d**, Network visualization of fibrosis-related Gene Ontology terms ($n = 91$). Dots indicate genes that were upregulated in CD44^{hi}CD69^{lo} (green), CD44^{hi}CD69^{hi}CD103^{lo} (red) and CD44^{hi}CD69^{hi}CD103^{hi} T cells (blue), compared with CD44^{lo} T cells. **e**, Heat map depicting fibrosis-related genes that were substantially upregulated among four groups of CD4$^+$ T cells in the lungs of *Asp*-Ag mice. **f**, Numbers of genes encoding fibrosis-related factors in each pathway among four groups of CD4$^+$ T cells in the lungs of *Asp*-Ag mice.

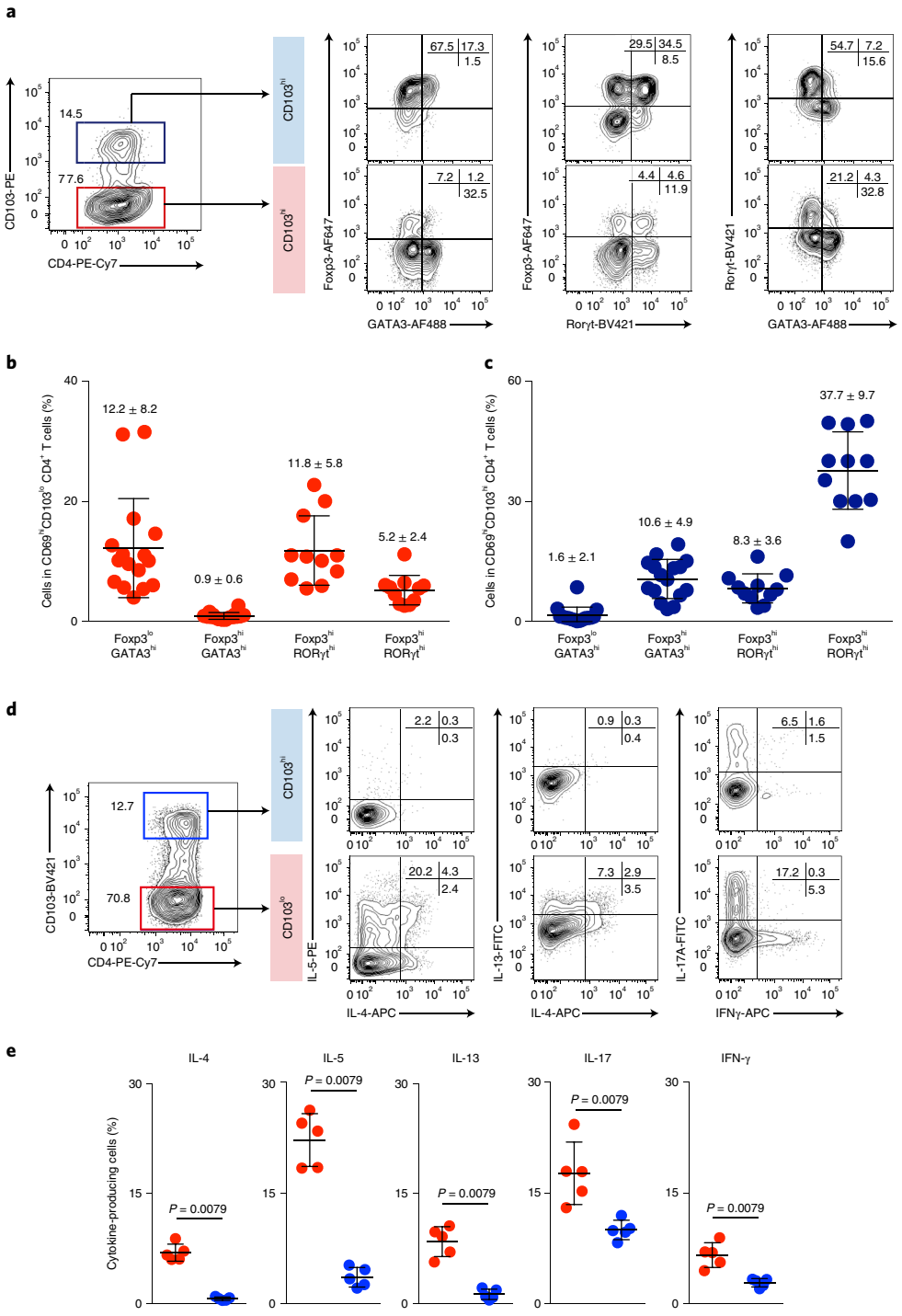

Fig. 3 | CD69^{hi}CD103^{lo} CD4$^+$ T cells were the effector cytokine producers in the inflamed lung. a, Representative intracellular staining profiles of Foxp3, GATA3 and Rorγt in CD69^{hi}CD103^{hi} CD4$^+$ T_{reg} cells (top) and CD69^{hi}CD103^{lo} CD4$^+$ T cells (bottom) in the lungs of *Asp*-Ag mice. More than three independent experiments were performed, with similar results. **b**,**c**, Pooled data of intracellular staining profiles of Foxp3, GATA3 and Rorγt in CD69^{hi}CD103^{lo} CD4$^+$ T cells (**b**) and CD69^{hi}CD103^{hi} CD4$^+$ T_{reg} cells (**c**) in the lungs of *Asp*-Ag wild-type mice ($n = 16$ samples stained with Foxp3 and GATA3; $n = 11$ samples stained with Foxp3 and Rorγt). Data represent means ± s.d. **d**, Representative intracellular staining profiles of IL-5, IL-4, IL-13, IFN-γ and IL-17 in CD69^{hi}CD103^{hi} CD4$^+$ T_{reg} cells (top) and CD69^{hi}CD103^{lo} CD4$^+$ T cells (bottom) in the lungs of *Asp*-Ag mice. More than three independent experiments were performed, with similar results. **e**, Percentages of the indicated cytokines in CD69^{hi}CD103^{lo} CD4$^+$ T cells (red) and CD69^{hi}CD103^{hi} CD4$^+$ T_{reg} cells (blue) in the lungs of *Asp*-Ag mice. The findings of five pooled independent experiments are shown. Data represent means ± s.d. *P* values were calculated by two-sided Mann–Whitney *U*-test.

and 12% expressed Rorγt (the master regulator of T_H17 cells) (Fig. 3a,b and Supplementary Fig. 4a), with few cells co-expressing GATA3 or Rorγt together with Foxp3 (the master regulator of T_{reg} cells) (0.9 and 5.2%, respectively). In contrast, between 60 and 80% of CD69^{hi}CD103^{hi} T cells expressed Foxp3, with approximately 50% of these co-expressing Rorγt, and 10% co-expressing

GATA3 (Fig. 3a,c and Supplementary Fig. 4b). On stimulation with phorbol 12-myristate 13-acetate (PMA) and ionomycin for 4 h, CD69^{hi}CD103^{lo} T cells exhibited significantly higher production of effector cytokines, such as IL-4, IL-5, IL-13, IL-17A and interferon-γ (IFN-γ), compared with CD69^{hi}CD103^{hi} T cells (Fig. 3d,e and Supplementary Fig. 4c). These results indicate that tissue-resident CD69^{hi}CD103^{lo} CD4$^+$ T cells produce effector cytokines in the *Aspergillus* antigen-induced chronically inflamed lung.

Foxp3$^+$ T$_{reg}$ cells suppress the pathology of chronic lung inflammation. Next, we investigated the immunological function of Foxp3$^+$ CD4$^+$ T cells during chronic lung inflammation. *Foxp3*^{DTR} mice, which express the diphtheria toxin receptor (DTR) under the control of the *Foxp3* gene locus, were repeatedly exposed to *Aspergillus* antigen followed by intranasal administration of *Diphtheria* toxin to deplete Foxp3^{hi} CD4$^+$ T cells (Supplementary Fig. 5a). The intranasal administration of *Diphtheria* toxin resulted in a significant decrease of Foxp3^{hi} CD4$^+$ T cells in the lung, but not in the spleen (Supplementary Fig. 5b,c). As expected, the percentage of CD69^{hi}CD103^{hi} T cells was significantly decreased as a result of the deletion of Foxp3$^+$ CD4$^+$ T cells (Supplementary Fig. 5d). A co-expression network analysis showed alterations in the gene expression of the remaining CD69^{hi}CD103^{hi} T cells from the lungs of *Aspergillus* antigen-exposed *Foxp3*^{DTR} mice after the administration of *Diphtheria* toxin (Fig. 4a, right). The remaining CD69^{hi}CD103^{hi} T cells showed increased expression of effector cytokine genes, such as *Il4*, *Il5*, *Il13* and *Ifng* (Fig. 4a, boxes in right panel), accompanied by an increase in the Foxp3^{lo}GATA3^{hi} cell subpopulation (Fig. 4b and Supplementary Fig. 5e) The administration of *Diphtheria* toxin also resulted in a significant increase in CD103^{lo}Foxp3^{lo}GATA3^{hi} T cells and a significant decrease in CD103^{lo}Foxp3^{lo}Rorγt^{hi} T cells (Supplementary Fig. 5f,g). CD69^{hi}CD103^{hi} T cells in *Foxp3*^{DTR} mice showed enhanced expression of IL-5 and IL-13 (Fig. 4c and Supplementary Fig. 5h). A histological analysis of the lungs of *Foxp3*^{DTR} mice revealed a further increase in the infiltration of inflammatory cells around the bronchi (Fig. 4d). The absolute numbers of infiltrating inflammatory cells in BAL fluid were significantly increased in *Foxp3*^{DTR} mice compared with wild-type mice (Fig. 4e). *Foxp3*^{DTR} mice showed substantially higher levels of fibrosis compared with those in control groups, as assessed by Sirius Red staining and collagen levels (Fig. 4f,g). These results indicate that Foxp3$^+$ T$_{reg}$ cells suppress the pathology of *Aspergillus* antigen-induced chronic inflammation in the lung. Moreover, we investigated whether Foxp3$^+$Rorγt$^+$ T$_{reg}$ cells regulated the *Aspergillus* antigen-induced lung inflammation in vivo (Supplementary Fig. 5i,j). *Rorc*$^{fl/fl}$*Foxp3*-cre mice showed similar numbers of infiltrating inflammatory cells in BAL fluid compared with those in *Rorc*$^{fl/fl}$ mice after the administration of *Aspergillus* antigen for 7 weeks (Fig. 4h). These data indicate that Foxp3$^+$Rorγt$^+$ T$_{reg}$ cells do not contribute to the suppression of *Aspergillus* antigen-induced chronic inflammation in the lung.

Global views of the chromatin landscapes in CD103^{lo} T$_{RM}$ and CD103^{hi} tissue-resident T$_{reg}$ cells reveal their differential regulomes. To assess whether the tissue-resident CD44^{hi}CD69^{hi} CD4$^+$ T cells induced by chronic *Aspergillus* antigen exposure are CD4$^+$ T$_{RM}$ cells, we performed parabiosis experiments using Thy1.1 and Thy1.2 mice that were subjected to a 7-week challenge with *Aspergillus* antigen followed by a 7-week rest period to allow memory T cell formation (Fig. 5a). Pairs of naive Thy1.1 mice and allergen-challenged Thy1.2 mice with a 7-week rest period were surgically joined, and the pairs of mice were analyzed 2 weeks later. After intravenous staining with anti-CD4 antibody, we found that congenically marked CD4$^+$ T cells were mixed, almost equivalently, in the circulating CD4$^+$ T cells of both the naive and challenged parabionts (Fig. 5b,c). In contrast, in the tissue-resident CD4$^+$ T cells, the population of Thy1.2$^+$ cells in the lungs of the challenged Thy1.2 parabionts was significantly larger than that in the naive Thy1.1 parabionts. These parabiosis experiments using mice with a 7-week rest period indicate that chronic *Aspergillus* antigen exposure induced CD4$^+$ T$_{RM}$ cells (Fig. 5b,c).

Analysis of chromatin accessibility can give detailed and highly informative data about gene regulation and the functional state of cells. We performed an assay to detect transposase-accessible chromatin using sequencing (ATAC-Seq), using lung CD4$^+$ T cells recovered from mice subjected to a 7-week *Aspergillus* antigen challenge with a 7-week rest period (Fig. 6a and Supplementary Fig. 6a). A gating strategy based on the expression of CD44, CD69 and CD103 was again used (see Fig. 2a, top). Principal component analysis revealed that each subpopulation of CD4$^+$ T cells exhibited a distinct regulome profile (Fig. 6b). Among a total of 26,449 accessible regulatory elements from four subpopulations of CD4$^+$ T cells in the lung, approximately 37% were common to all subpopulations, whereas the majority (63%) of the regions were either unique to a single subpopulation (CD69^{hi}CD103^{lo} T cell-specific region: 7.93%; CD69^{hi}CD103^{hi} T cell-specific region: 11.00%) or shared by two subpopulations of CD4$^+$ T cells (common region: 11.39%) (Fig. 6c). The enrichment of consensus transcription factor motifs showed that specific transcription factors were differentially enriched in each subpopulation of CD4$^+$ T cells (Supplementary Fig. 6b). For example, Tcf7 and Lef1 were enriched in CD44^{lo} T cells, and Stat6 and GATA3 were enriched in CD44^{hi}CD69^{hi}CD103^{lo} T cells, whereas Foxp3 was enriched in CD44^{hi}CD69^{hi}CD103^{hi} T cells. More importantly, we found that the signature genes in each subpopulation were epigenetically regulated (Fig. 6d–f). For example, the regulatory elements of effector cytokines such as *Il4*, *Il13* and *Il17a*, which were ranked in the top 10% (Fig. 6d, left), were preferentially accessible in CD44^{hi}CD69^{hi}CD103^{lo} T cells (Supplementary Fig. 6c,d). In contrast, regulatory elements of *Foxp3* and *Itgae*, which were ranked in top 10% (Fig. 6e, left), were selectively accessible in CD44^{hi}CD69^{hi}CD103^{hi} T cells (Supplementary Fig. 6e,f). The specific regulatory elements of fibrosis-related genes were highly accessible in both CD44^{hi}CD69^{hi}CD103^{lo} and CD44^{hi}CD69^{hi}CD103^{hi} CD4$^+$ T cells compared with CD44^{lo} or CD44^{hi}CD69^{lo} CD4$^+$ T cells (Fig. 6g and Supplementary Fig. 6g,h). More importantly, the enriched pathways of the fibrosis-related genes revealed by ATAC-Seq were similar to those identified by RNA-Seq analysis. Thus, high-resolution profiling of chromatin landscapes by ATAC-Seq identified subpopulation-specific regulatory elements near genes that may specify the function of CD44^{hi}CD69^{hi}CD103^{lo} and CD44^{hi}CD69^{hi}CD103^{hi} T cells.

Tissue-resident CD4$^+$ T cells in the lungs shape the inflammation accompanied by fibrotic responses. Next, we investigated the pathophysiological roles of CD103^{lo} T$_{RM}$ cells and CD103^{hi} tissue-resident T$_{reg}$ cells in vivo. Mice subjected to the 7-week *Aspergillus* antigen challenge followed by a 7-week rest period were rechallenged with a single dose of antigen, and the infiltration of inflammatory cells in BAL fluid was found to be increased compared with that in mice without the antigen rechallenge in vivo (Fig. 7a and Supplementary Fig. 7a). Increased infiltration of inflammatory cells in the lung parenchyma, and enhanced collagen deposition around the bronchi, were also observed 24 and 48 h after rechallenge of *Aspergillus* antigen (Supplementary Fig. 7b,c).

To prevent T cells from repositioning from secondary lymphoid organs to the tissue, we administered FTY720 (ref. [38]) (Supplementary Fig. 7d). As expected, FTY720 treatment resulted in a dramatic decrease in CD4$^+$ T cells in the peripheral blood mononuclear cells (Fig. 7b). FTY720 treatment followed by a single *Aspergillus* antigen challenge induced a significant decrease of circulating CD4$^+$ T cells, but not in tissue-resident CD4$^+$ T cells in the lungs (Fig. 7c). At the same time, comparable numbers of inflammatory cells infiltrated in

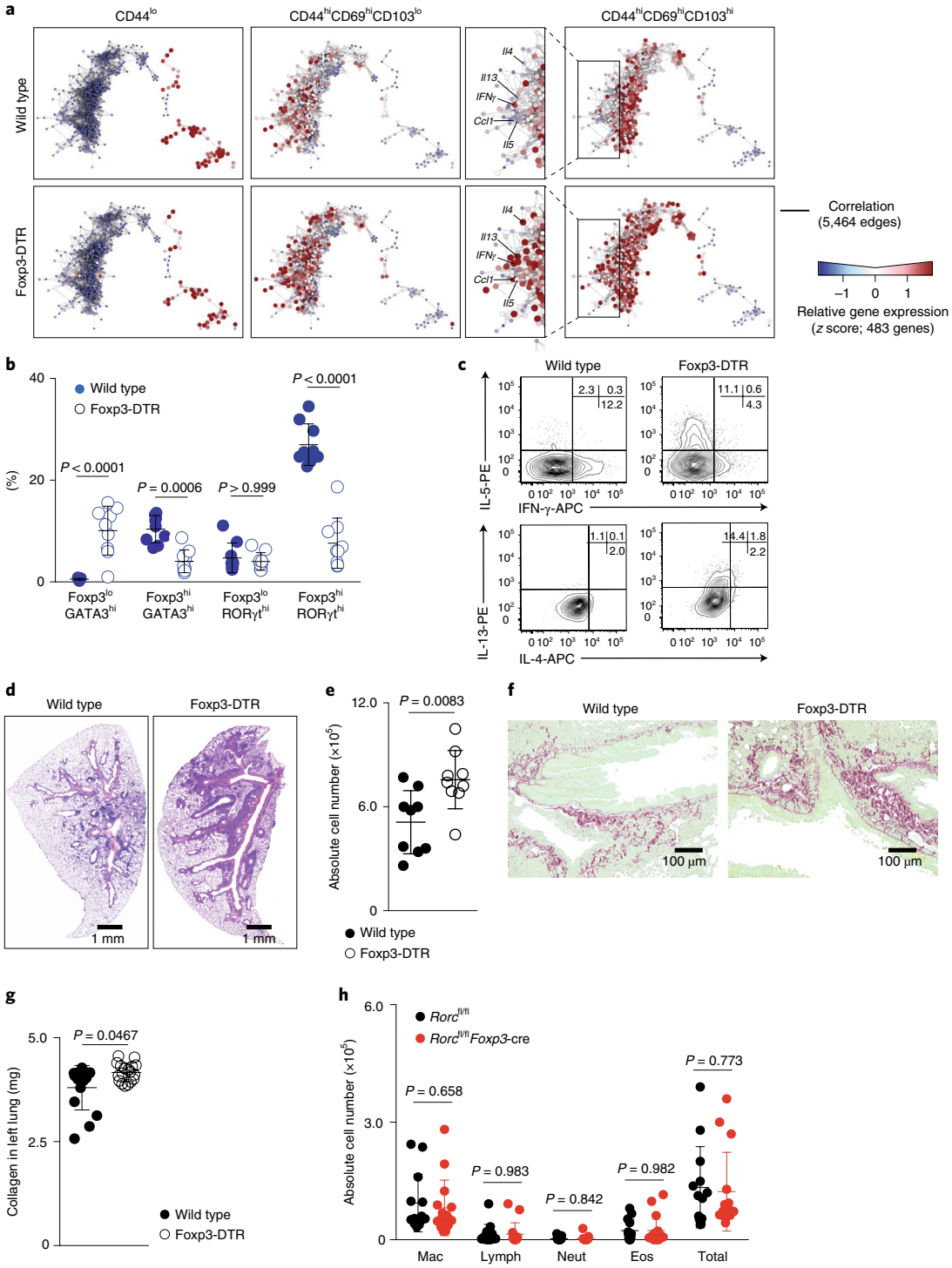

Fig. 4 | Depletion of Foxp3$^+$ CD4$^+$ T$_{reg}$ cells resulted in exacerbation of chronic lung inflammation. a, Relative gene expression profiles in the co-regulation network in naive CD44^{lo}CD69^{lo} (left), CD69^{hi}CD103^{lo} CD4$^+$ (middle) and CD69^{hi}CD103^{hi} CD4$^+$ T cells (right) from the lungs of *Asp*-Ag wild-type mice (BALB/c background) (top) and Foxp3-DTR transgenic mice (bottom). **b**, Intracellular staining profiles of Foxp3, GATA3 and Rorγt in CD69^{hi}CD103^{hi} CD4$^+$ T cells in the lungs of *Asp*-Ag wild-type mice ($n = 9$) and Foxp3-DTR transgenic mice ($n = 9$). **c**, Intracellular staining profiles of IFN-γ and IL-5 (top) and IL-13 and IL-4 (bottom) in CD69^{hi}CD103^{hi} CD4$^+$ T cells in the lungs of *Asp*-Ag wild-type mice (left) and Foxp3-DTR transgenic mice (right). Three independent experiments were performed, with similar results. **d**, Representative histological sections of the lungs from *Asp*-Ag wild-type mice and Foxp3-DTR transgenic mice. Sections were stained with hematoxylin and eosin. More than nine mice per group were analyzed. **e**, Total numbers of cells in the BAL fluid from *Asp*-Ag wild-type ($n = 9$) and Foxp3-DTR transgenic mice ($n = 9$). **f**, Representative histological sections of lungs from *Asp*-Ag wild-type (left) and Foxp3-DTR transgenic mice (right). Sections were stained with Sirius Red. More than nine mice per group were analyzed. **g**, Quantification of collagen protein in the lungs from *Asp*-Ag wild-type ($n = 15$) and Foxp3-DTR transgenic mice ($n = 18$). **h**, Absolute numbers of total cells (Total), macrophages (Mac), eosinophils (Eos), neutrophils (Neut) and lymphocytes (Lymph) in BAL fluid from *Asp*-Ag *Rorc*$^{fl/fl}$ (C57BL/6J background; $n = 13$) and *Rorc*$^{fl/fl}$*Foxp3*-cre mice ($n = 15$). Data are represented as means ± s.d. *P* values were calculated by two-way ANOVA (**b**) or two-sided Mann–Whitney *U*-test (**e**, **g** and **h**).

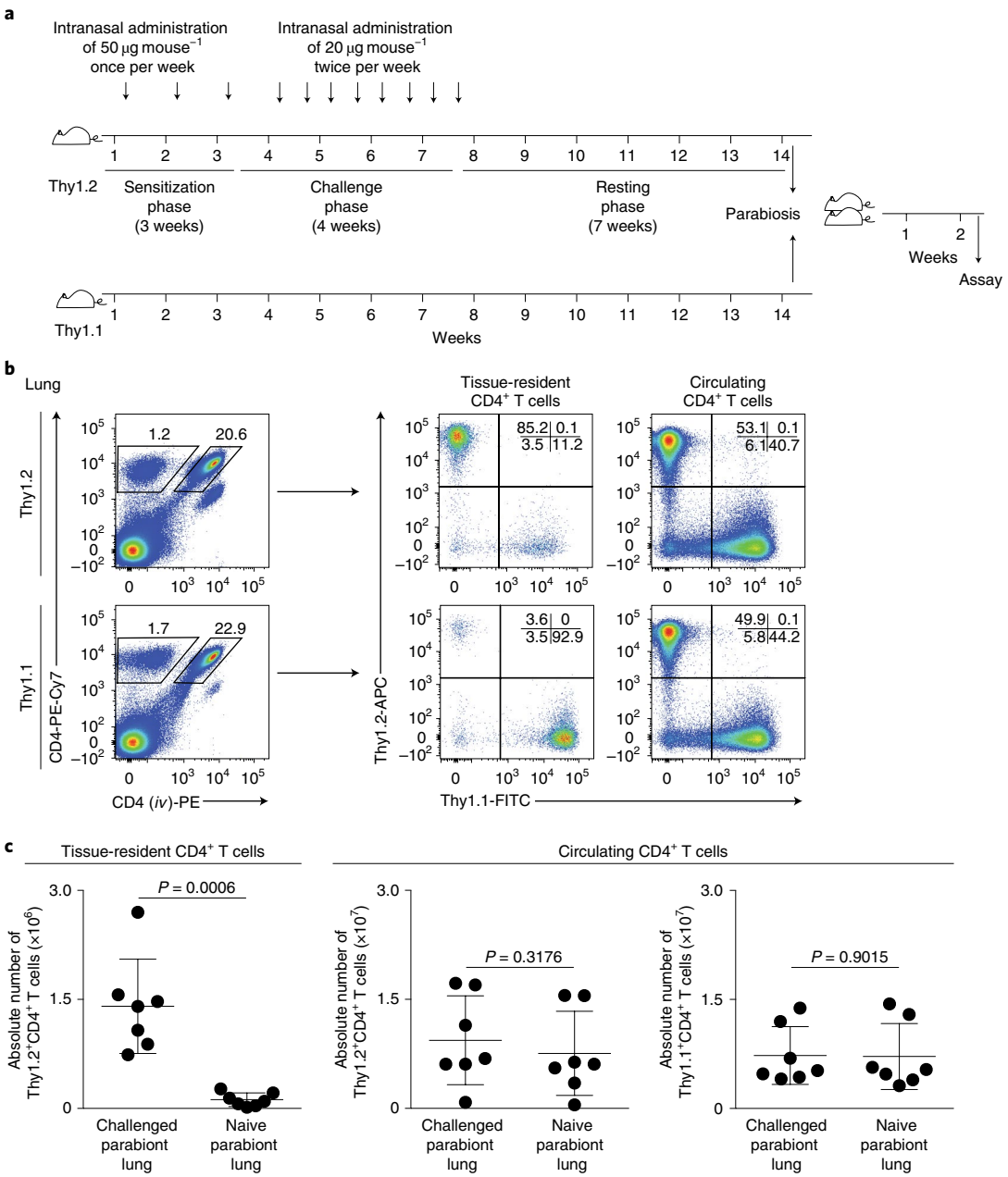

Fig. 5 | CD4$^+$ T_{RM} cells were induced by chronic *Aspergillus* antigen exposure. a, Schematic of the experimental protocol. Mice were repeatedly exposed to *Aspergillus* antigen for 7 weeks, with a 7-week rest period followed by the parabiosis experiment. **b**, Representative plots of cell-surface staining of anti-Thy1.1 and anti-Thy1.2 in tissue-resident CD4$^+$ T cells (left) and circulating CD4$^+$ T cells (right) in the lungs from *Asp*-Ag Thy1.2 mice (top) and Thy1.1 mice (bottom). Three independent experiments were performed, with similar results. **c**, Absolute numbers of Thy1.2$^+$ CD4$^+$ T cells in the tissue-resident CD4$^+$ T cell population (left), Thy1.2$^+$ CD4$^+$ T cells in the circulating CD4$^+$ T cell population (middle) and Thy1.1$^+$ CD4$^+$ T cells in the circulating CD4$^+$ T cell population (right) from the lungs of *Asp*-Ag Thy1.2 (challenged parabiont lung) and Thy1.1 mice (naive parabiont lung) ($n = 7$ mice per group). Data represent means ± s.d. *P* values in were calculated by two-sided Mann–Whitney *U*-test.

the BAL fluid, accompanied by fibrotic responses in the lungs of the mice with FTY720 treatment (Fig. 7d,e). These results indicate that lung inflammation induced by rechallenge of the *Aspergillus* antigen was induced by CD4$^+$ T_{RM} cells.

Finally, we performed a set of experiments using the administration of FTY720 and a single challenge of *Aspergillus* antigen, with or without intraperitoneal injection of anti-CD103 antibodies (Supplementary Fig. 7e). The administration of anti-CD103 antibodies resulted in a substantial depletion of CD44^{hi}CD69^{hi}CD103^{hi} circulating CD4$^+$ T cells (Supplementary Fig. 7f,g). The administration of a single dose of *Aspergillus* antigen to mice that received anti-CD103 antibody treatment resulted in exacerbation of lung inflammation, accompanied by increased inflammatory cell infiltration and fibrotic responses compared with mice treated with control antibodies (Fig. 7f,g). Thus, the CD103^{hi} subpopulation of CD44^{hi}CD69^{hi} CD4$^+$ T cells constrains lung inflammation and the extent of fibrotic responses.

Discussion

We have demonstrated that repeated fungal exposure induced lung inflammation and fibrotic responses, and the presence of two functionally distinct CD4 T_{RM} populations in the lung. CD69^{hi}CD103^{lo}

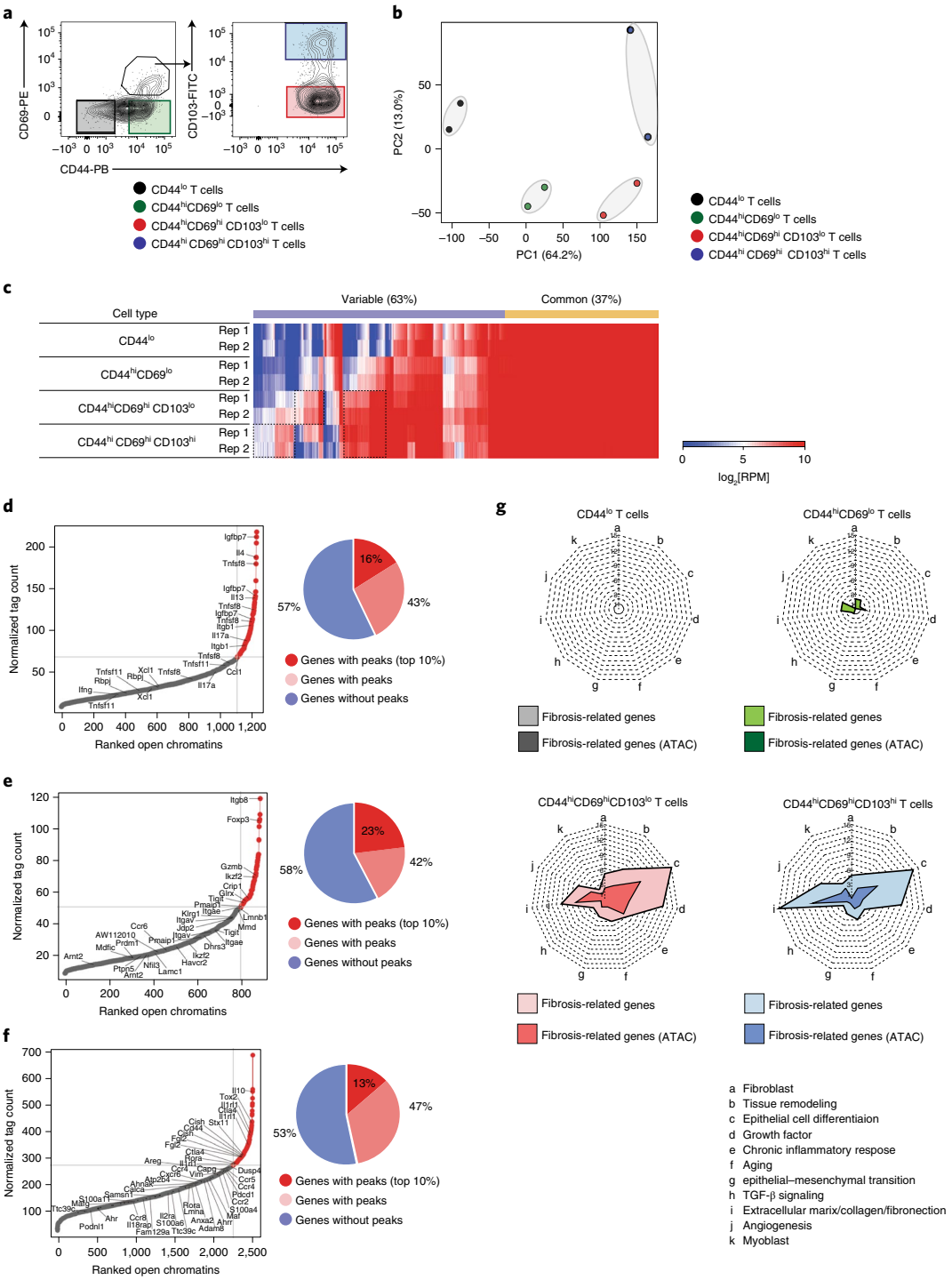

Fig. 6 | CD44^{hi}CD69^{hi} CD4^{+} T$_{RM}$ regulomes show fibrotic features. a, Cell-sorting strategy for the four groups of CD4^{+} T cells in the lungs of *Asp*-Ag mice subjected to a 7-week *Aspergillus* antigen challenge followed by a 7-week rest period (Supplementary Fig. 5a). **b**, Principal component analysis plots of ATAC-Seq data from the four groups of CD4^{+} T cells ($n=8$). Duplicates of pooled samples are shown. **c**, Comparison of global ATAC peaks in the four groups of CD4^{+} T cells in the lungs of mice subjected to a 7-week *Aspergillus* antigen challenge followed by a 7-week rest period. A heat map (right) shows the signal intensity (log_2[reads per million mapped reads (RPM)]) of each ATAC peak. Rep, replication. **d**–**f**, Left: cumulative normalized tag counts of ATAC peaks in the indicated regions (CD44^{hi}CD69^{hi}CD103^{lo} T-cell-specific region (**d**), CD44^{hi}CD69^{hi}CD103^{hi} T-cell-specific region (**e**) and the common region (**f**)), plotted against ranked open chromatins. Right: pie charts depict specific genes in the indicated regions with or without ATAC peaks ($n=27$ in **d**, $n=56$ in **e** and $n=60$ in **c**). **g**, Numbers of genes encoding fibrosis-related factors with ATAC peaks in each pathway among the four groups of CD4^{+} T cells in the lungs of *Asp*-Ag mice. The results are overwritten on the profiles shown in Fig. 2f.

CD4^{+} T$_{RM}$ cells produced effector cytokines such as IL-5 and IL-13, and were directly involved in the pathology of fungus-induced fibrotic responses in the lung. In contrast with the reported functions of CD103^{hi} CD8^{+} T$_{RM}$ cells[15], CD103^{hi} tissue-resident CD4^{+} T cells frequently expressed Foxp3, and depletion of Foxp3^{+} CD4^{+} T$_{reg}$ cells or CD103^{hi} CD4^{+} T cells resulted in enhanced fibrotic responses in

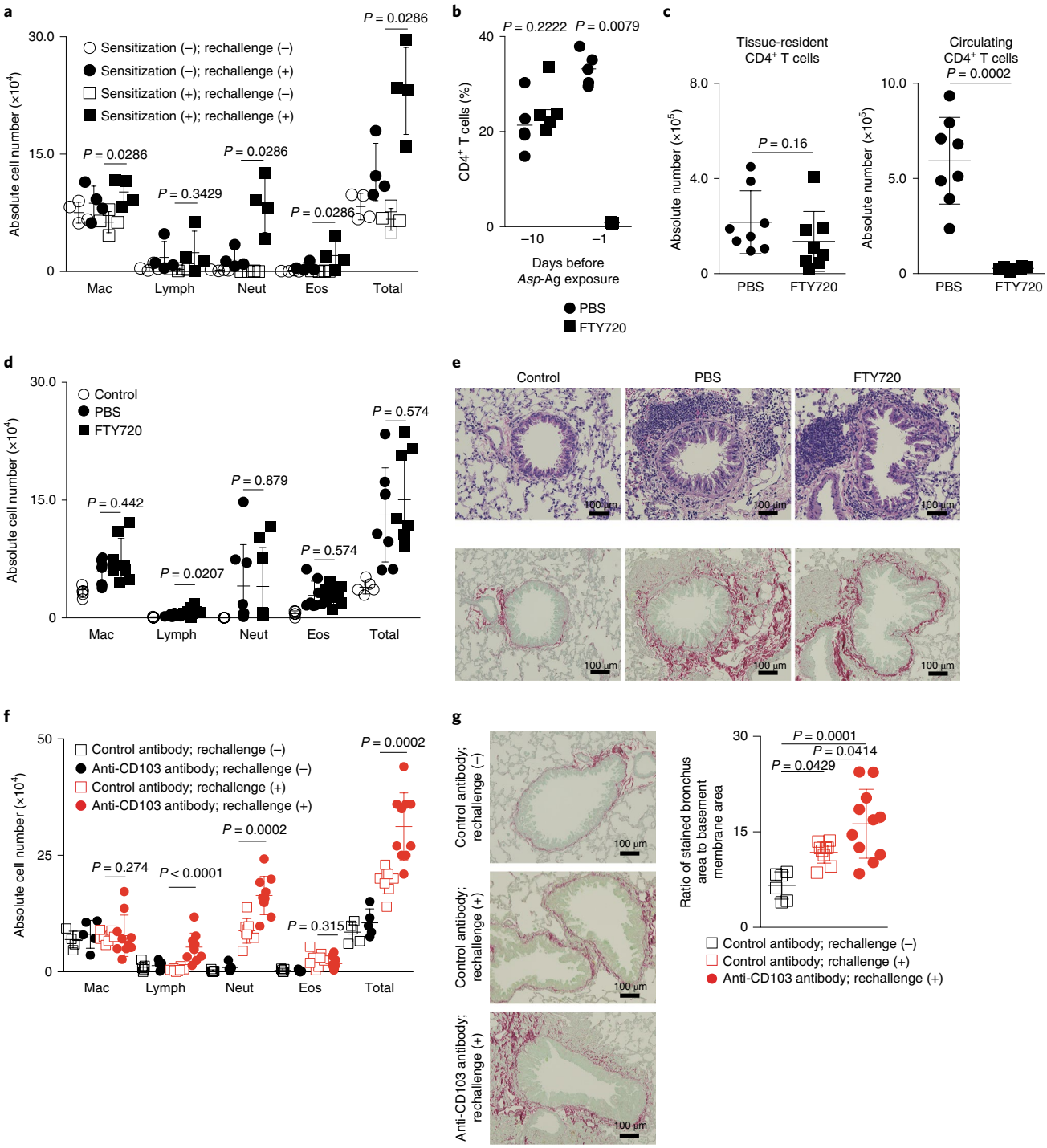

Fig. 7 | CD4⁺ T_{RM} cells are sufficient to induce lung inflammation accompanied by fibrotic responses. a, Absolute numbers of total cells, macrophages, eosinophils, neutrophils and lymphocytes in BAL fluid from four groups of mice (no sensitization and no rechallenge; no sensitization but rechallenge; sensitization but no rechallenge; and sensitization and rechallenge; $n = 4$ per group). **b**, Proportion of CD4⁺ T cells in peripheral blood mononuclear cells from PBS- ($n = 5$) and FTY720-treated mice ($n = 5$). **c**, Absolute numbers of tissue-resident T cells (left) and circulating T cells (right) in the lungs from PBS- and FTY720-treated *Asp*-Ag mice ($n = 8$ mice per group). **d**, Absolute numbers of total cells, macrophages, eosinophils, neutrophils and lymphocytes in BAL fluid from control mice ($n = 5$), PBS-treated mice ($n = 8$) and FTY720-treated mice ($n = 8$). **e**, Representative histological sections of lungs from control mice, PBS-treated mice and FTY720-treated mice. Sections were stained with hematoxylin and eosin (top) or Sirius Red (bottom). More than three mice per group were analyzed. **f**, Absolute numbers of total cells, macrophages, eosinophils, neutrophils and lymphocytes in BAL fluid from four groups of mice (control antibody with no rechallenge ($n = 5$); control antibody with rechallenge ($n = 8$); anti-CD103 antibody with no rechallenge ($n = 5$); and anti-CD103 antibody with rechallenge ($n = 10$)). **g**, Left: representative histology of mouse lung specimens stained with Sirius Red ($n = 2$ independent experiments). Right: ratios of areas of randomly selected regions stained with Sirius Red surrounding the bronchi versus areas of the associated basement membranes (control antibody with no rechallenge: $n = 6$ samples from $n = 3$ mice; control antibody with rechallenge: $n = 9$ samples from $n = 3$ mice; anti-CD103 antibody with rechallenge: $n = 11$ samples from $n = 4$ mice). Data represent means ± s.d. *P* values were calculated by two-sided Mann–Whitney *U*-test (**a**–**d** and **f**) or one-way ANOVA (**g**).

the lung. Moreover, we found that CD44^{hi}CD69^{hi}CD103^{lo} pathogenic effector CD4$^+$ T$_{RM}$ cells and CD44^{hi}CD69^{hi}CD103^{hi} tissue-resident CD4$^+$ T$_{reg}$ cells are transcriptionally, epigenetically and functionally distinct. Thus, this study highlights novel tissue-resident CD4$^+$ T cell populations in the chronically inflamed lung that play crucial roles in the establishment of fibrotic responses in the lung.

In the current study, we identified that the lung tissue-resident CD44^{hi}CD69^{hi} CD4$^+$ T cells induced by repeated exposure to fungal antigens consist of CD69^{hi}CD103^{lo} CD4$^+$ T$_{RM}$ cells and CD69^{hi}CD103^{hi} T$_{reg}$ cells, both of which showed enhanced expression of fibrosis-related genes compared with circulating CD44^{hi} naive or CD44^{hi}CD69^{lo} CD4$^+$ T cells. The fibrosis-related gene signature appeared to be acquired during the differentiation into tissue-resident CD4$^+$ T cells. Among the fibrosis-related genes upregulated in tissue-resident CD44^{hi}CD69^{hi} CD4$^+$ T cells, significant differences were observed between CD103^{lo} CD4$^+$ T$_{RM}$ cells and CD103^{hi} T$_{reg}$ cells. The profibrotic cytokine genes *Il5* and *Il13* were selectively expressed in CD69^{hi}CD103^{lo} CD4$^+$ T$_{RM}$ cells. In contrast, CD69^{hi}CD103^{hi}Foxp3$^+$ T$_{reg}$ cells expressed high levels of *Itgae* and *Foxp3* and constrained the fungal antigen-induced fibrotic responses in the inflamed lung. Interestingly, both *Itgae* and *Foxp3* are induced by the fibrosis-associated cytokine transforming growth factor-β (TGF-β), indicating that they may act as a rheostat limiting fibrotic responses. We identified CD69^{hi}CD103^{lo} CD4$^+$ T$_{RM}$ cells as a pathogenic cell population promoting massive lung inflammation with fibrotic responses after repeated exposure to fungal antigens. The CD69^{hi}CD103^{lo} CD4$^+$ T$_{RM}$ cells exhibited unique genome-wide transcriptomes and regulomes, with enhanced production of effector cytokines, including IL-4, IL-5, IL-13, IL-17A and IFN-γ. It has been reported that amphiregulin (encoded by *Areg*, and produced from pathogenic T$_H$2 cells) plays a crucial role in fibrotic responses in eosinophilic inflammation in the lung via the production of osteopontin by eosinophils[30]. Amphiregulin produced from T$_{reg}$ cells is also reported to be important for tissue repair processes[20,27,39]. In the current study, we found that both CD69^{hi}CD103^{lo} CD4$^+$ T$_{RM}$ and CD69^{hi}CD103^{hi} T$_{reg}$ cells expressed high levels of *Areg*. Although it is not known whether tissue repair processes occur in the current experimental model of fungus-induced inflammation, a profibrotic function of amphiregulin may play a distinct role. Importantly, the fibrosis-related genes upregulated in CD69^{hi}CD103^{hi} T$_{reg}$ cells were distinct from those upregulated in CD69^{hi}CD103^{lo} T$_{RM}$ cells. Blimp1 (encoded by *Prdm1*) is known to be crucial for both the appropriate function of T$_{reg}$ cells and stabilization of Foxp3 expression in T$_{reg}$ cells[40,41]. We found high expression of both *Foxp3* and *Prdm1* in CD69^{hi}CD103^{hi} T$_{reg}$ cells, which indicates an immunosuppressive role, rather than a profibrotic role, in the inflammatory tissue.

We demonstrated that repeated fungal antigen stimulation induced CD69^{hi}CD103^{hi} CD4$^+$ T cells, a substantial proportion of which were Foxp3^{hi}Rorγt^{hi} cells. Surprisingly, *Rorc* deletion in Foxp3-positive cells resulted in little impact on the extent of lung inflammation, which indicates that Foxp3^{hi}Rorγt^{hi} T$_{reg}$ cells might not have an inhibitory function in the lung inflammation induced by repetitive exposure to the *Aspergillus* antigen. In contrast, gut microbiota-induced Foxp3^{hi}Rorγt^{hi} T$_{reg}$ cells were reported to regulate type 2 immune responses in the intestine[19,42]. Although microbiota-induced Foxp3^{hi}Rorγt^{hi} CD4$^+$ T cells are maintained in the intestine under normal steady-state conditions, lung CD69^{hi}CD103^{hi}Foxp3^{hi}Rorγt^{hi} T$_{reg}$ cells were only detected after repeated exposure to fungal antigens. Thus, these two populations appeared to be induced by distinct mechanisms, and might have different functions in vivo, although both populations express Rorγt and Foxp3.

An important finding from the present study is that CD103 is a key molecule that can distinguish the function of lung CD4$^+$ T$_{RM}$ cells. CD103 is well appreciated as a key molecule for the epithelial localization of CD8$^+$ T$_{RM}$ cells[6,43]. The binding of CD103 to E-cadherin increases T cell adherence to epithelial cells[44], suggesting that CD103 may compartmentalize CD69^{hi}CD103^{hi} CD4$^+$ T cells from CD69^{hi}CD103^{lo} CD4$^+$ T$_{RM}$ cells within the mucosal tissue in the lung. In addition, the localization of CD69^{hi}CD103^{hi} CD4$^+$ T cells adjacent to epithelial cells may confer the suppressive function of CD69^{hi}CD103^{hi} CD4$^+$ T cells, because epithelial cells are known to be the main source of TGF-β in the lung[45]. At the same time, TGF-β is known to be important for upregulation of CD103 expression and repression of *Klf2* expression[35]. Indeed, CD69^{hi}CD103^{hi} CD4$^+$ T cells downregulated expression of *Klf2*. Interestingly, CD69^{hi}CD103^{hi} CD4$^+$ T cells also had high expression of *Klrg1*, which encodes KLRG1, another binding partner of E-cadherin[46]. Thus, tissue-localization in vivo may be closely related to the unique characteristics of tissue-resident CD4$^+$ T cell subpopulations.

Patients with severe persistent asthma and allergic bronchopulmonary aspergillosis often show airway remodeling, structural alterations of the airway wall (such as subepithelial thickening), vascular changes and fibrosis[47–49]. High sensitivity to fungi—especially to *Aspergillus*—increases the risk of adult-onset asthma[30]. Our findings indicate that CD4$^+$ T$_{RM}$ cells could be potential therapeutic targets for patients with chronic fungal inflammation and fibrotic responses.

In summary, we identified pathogenic and immunosuppressive tissue-resident CD4$^+$ T cell subpopulations (CD69^{hi}CD103^{lo} CD4$^+$ T$_{RM}$ cells and CD69^{hi}CD103^{hi}Foxp3$^+$ CD4$^+$ T$_{reg}$ cells, respectively) in the chronically inflamed lung with fibrotic responses. We have highlighted the epigenetically regulated functional dichotomy of the tissue-resident CD4$^+$ T cell subpopulations that govern the pathophysiology of the fungus-induced fibrotic responses. Understanding cellular and molecular mechanisms through which distinct tissue-resident CD4$^+$ T cells are generated will be essential for the development of new therapeutic strategies for intractable inflammation-associated fibrotic diseases.

Online content

Any methods, additional references, Nature Research reporting summaries, source data, statements of code and data availability and associated accession codes are available at https://doi.org/10.1038/s41590-019-0494-y.

Received: 30 May 2019; Accepted: 12 August 2019;
Published online: 07 October 2019

References

1. Manz, R. A., Hauser, A. E., Hiepe, F. & Radbruch, A. Maintenance of serum antibody levels. *Annu. Rev. Immunol.* **23**, 367–386 (2005).
2. Pulendran, B. & Ahmed, R. Immunological mechanisms of vaccination. *Nat. Immunol.* **12**, 509–517 (2011).
3. Sallusto, F., Geginat, J. & Lanzavecchia, A. Central memory and effector memory T cell subsets: function, generation, and maintenance. *Annu. Rev. Immunol.* **22**, 745–763 (2004).
4. Masopust, D. & Soerens, A. G. Tissue-resident T cells and other resident leukocytes. *Annu. Rev. Immunol.* **37**, 521–546 (2019).
5. Mueller, S. N. & Mackay, L. K. Tissue-resident memory T cells: local specialists in immune defence. *Nat. Rev. Immunol.* **16**, 79–89 (2016).
6. Gebhardt, T. et al. Memory T cells in nonlymphoid tissue that provide enhanced local immunity during infection with herpes simplex virus. *Nat. Immunol.* **10**, 524–530 (2009).
7. Kimura, M. Y. et al. Crucial role for CD69 in allergic inflammatory responses: CD69-Myl9 system in the pathogenesis of airway inflammation. *Immunol. Rev.* **278**, 87–100 (2017).
8. Sathaliyawala, T. et al. Distribution and compartmentalization of human circulating and tissue-resident memory T cell subsets. *Immunity* **38**, 187–197 (2013).
9. Watanabe, R. et al. Human skin is protected by four functionally and phenotypically discrete populations of resident and recirculating memory T cells. *Sci. Transl. Med.* **7**, 279ra39 (2015).
10. Park, C. O. & Kupper, T. S. The emerging role of resident memory T cells in protective immunity and inflammatory disease. *Nat. Med.* **21**, 688–697 (2015).
11. O'Shea, J. J. & Paul, W. E. Mechanisms underlying lineage commitment and plasticity of helper CD4$^+$ T cells. *Science* **327**, 1098–1102 (2010).

12. Sallusto, F., Cassotta, A., Hoces, D., Foglierini, M. & Lanzavecchia, A. Do memory CD4 T cells keep their cell-type programming: plasticity versus fate commitment? T-cell heterogeneity, plasticity, and selection in humans. *Cold Spring Harb. Perspect. Biol.* **10**, a029421 (2018).
13. Nakayama, T. et al. T_H2 cells in health and disease. *Annu. Rev. Immunol.* **35**, 53–84 (2017).
14. Arens, R. & Schoenberger, S. P. Plasticity in programming of effector and memory CD8 T-cell formation. *Immunol. Rev.* **235**, 190–205 (2010).
15. Cheuk, S. et al. CD49a expression defines tissue-resident $CD8^+$ T cells poised for cytotoxic function in human skin. *Immunity* **46**, 287–300 (2017).
16. Ganesan, A. P. et al. Tissue-resident memory features are linked to the magnitude of cytotoxic T cell responses in human lung cancer. *Nat. Immunol.* **18**, 940–950 (2017).
17. Laidlaw, B. J. et al. $CD4^+$ T cell help guides formation of $CD103^+$ lung-resident memory $CD8^+$ T cells during influenza viral infection. *Immunity* **41**, 633–645 (2014).
18. Iijima, N. & Iwasaki, A. T cell memory. A local macrophage chemokine network sustains protective tissue-resident memory CD4 T cells. *Science* **346**, 93–98 (2014).
19. Ohnmacht, C. et al. The microbiota regulates type 2 immunity through $ROR\gamma t^+$ T cells. *Science* **349**, 989–993 (2015).
20. Arpaia, N. et al. A distinct function of regulatory T cells in tissue protection. *Cell* **162**, 1078–1089 (2015).
21. Panduro, M., Benoist, C. & Mathis, D. Tissue T_{reg}s. *Annu. Rev. Immunol.* **34**, 609–633 (2016).
22. Endo, Y., Hirahara, K., Yagi, R., Tumes, D. J. & Nakayama, T. Pathogenic memory type T_H2 cells in allergic inflammation. *Trends Immunol.* **35**, 69–78 (2014).
23. Islam, S. A. et al. Mouse CCL8, a CCR8 agonist, promotes atopic dermatitis by recruiting $IL\text{-}5^+$ T_H2 cells. *Nat. Immunol.* **12**, 167–177 (2011).
24. Mitson-Salazar, A. et al. Hematopoietic prostaglandin D synthase defines a proeosinophilic pathogenic effector human T_H2 cell subpopulation with enhanced function. *J. Allergy Clin. Immunol.* **137**, 907–918 e9 (2016).
25. Seumois, G. et al. Transcriptional profiling of T_H2 cells identifies pathogenic features associated with asthma. *J. Immunol.* **197**, 655–664 (2016).
26. Wambre, E. et al. A phenotypically and functionally distinct human T_H2 cell subpopulation is associated with allergic disorders. *Sci. Transl. Med.* **9**, eaam9171 (2017).
27. Morimoto, Y. et al. Amphiregulin-producing pathogenic memory T helper 2 cells instruct eosinophils to secrete osteopontin and facilitate airway fibrosis. *Immunity* **49**, 134–150.e6 (2018).
28. Wuthrich, M., Deepe, G. S. Jr. & Klein, B. Adaptive immunity to fungi. *Annu. Rev. Immunol.* **30**, 115–148 (2012).
29. Knutsen, A. P. et al. Fungi and allergic lower respiratory tract diseases. *J. Allergy Clin. Immunol.* **129**, 280–291 (2012)
30. Jaakkola, M. S., Ieromnimon, A. & Jaakkola, J. J. Are atopy and specific IgE to mites and molds important for adult asthma? *J. Allergy Clin. Immunol.* **117**, 642–648 (2006).
31. Eming, S. A., Wynn, T. A. & Martin, P. Inflammation and metabolism in tissue repair and regeneration. *Science* **356**, 1026–1030 (2017).
32. Anderson, K. G. et al. Cutting edge: intravascular staining redefines lung CD8 T cell responses. *J. Immunol.* **189**, 2702–2706 (2012).
33. Van der Maaten, L. & Hinton, G. Visualizing data using *t*-SNE. *J. Mach. Learn. Res.* **9**, 2579–2605 (2008).
34. Sakaguchi, S., Miyara, M., Costantino, C. M. & Hafler, D. A. $FOXP3^+$ regulatory T cells in the human immune system. *Nat. Rev. Immunol.* **10**, 490–500 (2010).
35. Skon, C. N. et al. Transcriptional downregulation of S1pr1 is required for the establishment of resident memory $CD8^+$ T cells. *Nat. Immunol.* **14**, 1285–1293 (2013).
36. Bromley, S. K., Thomas, S. Y. & Luster, A. D. Chemokine receptor CCR7 guides T cell exit from peripheral tissues and entry into afferent lymphatics. *Nat. Immunol.* **6**, 895–901 (2005).
37. Durek, P. et al. Epigenomic profiling of human $CD4^+$ T cells supports a linear differentiation model and highlights molecular regulators of memory development. *Immunity* **45**, 1148–1161 (2016).
38. Hondowicz, B. D. et al. Interleukin-2-dependent allergen-specific tissue-resident memory cells drive asthma. *Immunity* **44**, 155–166 (2016).
39. Ito, M. et al. Brain regulatory T cells suppress astrogliosis and potentiate neurological recovery. *Nature* **565**, 246–250 (2019).
40. Cretney, E. et al. The transcription factors Blimp-1 and IRF4 jointly control the differentiation and function of effector regulatory T cells. *Nat. Immunol.* **12**, 304–311 (2011).
41. Garg, G. et al. Blimp1 prevents methylation of Foxp3 and loss of regulatory T cell identity at sites of inflammation. *Cell Rep.* **26**, 1854–1868.e5 (2019).
42. Sefik, E. et al. Individual intestinal symbionts induce a distinct population of $ROR\gamma^+$ regulatory T cells. *Science* **349**, 993–997 (2015).
43. Cepek, K. L. et al. Adhesion between epithelial cells and T lymphocytes mediated by E-cadherin and the alpha E beta 7 integrin. *Nature* **372**, 190–193 (1994).
44. Lee, Y. T. et al. Environmental and antigen receptor-derived signals support sustained surveillance of the lungs by pathogen-specific cytotoxic T lymphocytes. *J. Virol.* **85**, 4085–4094 (2011).
45. Makinde, T., Murphy, R. F. & Agrawal, D. K. The regulatory role of TGF-β in airway remodeling in asthma. *Immunol. Cell Biol.* **85**, 348–356 (2007).
46. Van den Bossche, J., Malissen, B., Mantovani, A., De Baetselier, P. & Van Ginderachter, J. A. Regulation and function of the E-cadherin/catenin complex in cells of the monocyte-macrophage lineage and DCs. *Blood* **119**, 1623–1633 (2012).
47. Lambrecht, B. N. & Hammad, H. The airway epithelium in asthma. *Nat. Med.* **18**, 684–692 (2012).
48. Foster, P. S. et al. Modeling T_H2 responses and airway inflammation to understand fundamental mechanisms regulating the pathogenesis of asthma. *Immunol. Rev.* **278**, 20–40 (2017).
49. Greenberger, P. A. et al. Allergic bronchopulmonary aspergillosis. *J. Allergy Clin. Immunol. Pract.* **2**, 703–708 (2014).

Acknowledgements

We are grateful to Y. Kanno for critically reading and providing valuable suggestions on the manuscript. We are grateful to N. Iijima and K. J. Ishii for providing valuable suggestions on the parabiosis surgery. We are grateful to N. Takayama and K. Eto for providing valuable suggestions on the ATAC-Seq experiments. We thank T. Ito, K. Sugaya, M. Kato and T. Wada for excellent technical assistance. This work was supported by the following grants: Ministry of Education, Culture, Sports, Science and Technology Grants-in-Aid for Scientific Research (S) 26221305, JP19H05650, (C) 17K08876, 18K07164 and 19K16683; Practical Research Project for Allergic Diseases and Immunology (Research on Allergic Diseases and Immunology) from AMED (numbers JP19ek0410060 and JP19ek0410045); AMED-PRIME, AMED (number JP19gm6110005); AMED-CREST, AMED (number JP19gm1210003); the Mochida Memorial Foundation for Medical and Pharmaceutical Research, The Ichiro Kanehara Foundation for the Promotion of Medical Sciences and Medical Care; the Naito Foundation and the Takeda Science Foundation.

Author contributions

T.I., K. Hirahara and T.N. conceived of and designed the experiments. T.I., K. Hirahara, K.K., M.K., A.A., Y.M., J.K., A.O. and N.M. performed the experiments. T.I., K. Hirahara, K.K., M.K., A.O., D.J.T., Y.G., K. Hagiwara, Y.I., T.S., K.T. and T.N. analyzed and interpreted the data. T.I., K. Hirahara, D.J.T. and T.N. wrote, reviewed and edited the paper.

Competing interests

The authors declare no competing interests.

Additional information

Supplementary information is available for this paper at https://doi.org/10.1038/s41590-019-0494-y.

Correspondence and requests for materials should be addressed to T.N.

Peer review information Zoltan Fehervari was the primary editor on this article and managed its editorial process and peer review in collaboration with the rest of the editorial team.

Reprints and permissions information is available at www.nature.com/reprints.

Publisher's note Springer Nature remains neutral with regard to jurisdictional claims in published maps and institutional affiliations.

© The Author(s), under exclusive licence to Springer Nature America, Inc. 2019

Methods

Mice. The animals used in this study were backcrossed to C57BL/6J or BALB/cAJcl mice more than ten times. Collagen 1a2-GFP transgenic mice (C57BL/6J background) have been reported previously[50]. 'Depletion of regulatory T cell' (DEREG) mice (BALB/cAJcl background) were provided by T. Sparwasser (Johannes Gutenberg University). Foxp3-YFP-IRES-Cre mice (C57BL/6J background) were provided by A. Y. Rudensky (Memorial Sloan Kettering Cancer Center)[51]. All mice were used at 6–8 weeks of age and were maintained under specific-pathogen-free conditions. BALB/cAJcl, BALB/c *Foxn1*^{nu} and C57BL/6J mice were purchased from CLEA Japan. *Rorc*$^{fl/fl}$ mice (C57BL/6J background) were purchased from The Jackson Laboratory. All of the *Rorc*$^{fl/fl}$ and Foxp3-YFP-IRES-Cre mice used in this study were male. The DREG mice used in this study were both male and female. All other mice used in this study were female. Same-sex littermates were randomly assigned to experimental groups. The research proposals were reviewed by the ethics committee for animals at Chiba University (registration numbers 29–98 and 29–99).

Induction of chronic lung inflammation by repeated intranasal administration of *Aspergillus* antigen. *A. fumigatus* antigen (Greer) was administered intranasally for 7 weeks in a modified protocol based on the protocol described by Kerzerho et al.[52]. For the first 3 weeks, 50 µg of antigen was administered once a week. For the following 4 weeks, 20 µg of antigen was administered twice a week. In some experiments, mice were analyzed 7 weeks after the last antigen administration. Assays were performed 24 h after the last antigen administration.

Histology and immunofluorescence. Pathological changes were evaluated by hematoxylin and eosin, periodic acid–Schiff, Sirius Red and immunofluorescence staining, as previously described[53,54]. Cryostat sections of the lungs were stained and mounted with Fluorescent Mounting Medium (DakoCytomation). All immunofluorescence and histological analyses were carried out with a confocal laser microscope (LSM710; Carl Zeiss). Anti-CD4 (RM4-5; 552775; BD), anti-CD3e (2C11; 12-0031-82; eBioscience), anti-CD69 (AF2386; R&D Systems) and anti-type l collagen (LB-1102; LSL-LB-1102; LSL) were used for staining lung samples.

Isolation of CD4$^+$ T cells from the lung. After euthanasia, mice were perfused with 5 ml cold phosphate buffered saline (PBS) solution through the left and right ventricle, respectively. Lungs were dissociated in a C tube (Miltenyi Biotec) in digestion buffer (RPMI 1640 supplemented with collagenase type III (200 U ml^{-1}; Worthington) and DNase I (200 µg ml^{-1}; Sigma–Aldrich)) using a gentleMACS tissue dissociator (Miltenyi Biotec). After 30 min at 37 °C, samples were treated with final gentleMACS dissociation. Cell suspensions were passed through a 70-µm cell strainer (Greiner Bio-One). Lung mononuclear cells were separated using by Percoll solution (GE Healthcare).

Ex vivo analysis of CD4$^+$ T cells from the inflamed lung. Anti-CD3ε (145-2C11; 553061; BD), anti-CD4 (RM4-5; 552775; BD), anti-CD8a (53-6.7; 100725; BioLegend), anti-CD44 (IM7; 103020; Biolegend), anti-CD62L (MEL-14; 553150, 553152 and 560514; BD), anti-TCRβ (H57-597; 553174; BD), anti-CD69 (H1.2F3; 561932 and 560689; BD), anti-CD103 (2E7; 121421; BioLegend; and M290; 557494 and 557495; BD), anti-CD25 (PC61; 553866 and 561048; BD), anti-CD122 (IL-2Rβ; TM-Beta 1; 553362 and 564762; BD), anti-CD127 (IL7Rα; SB/199; 552543 and 564175; BD), anti-CD30L (RM153; 559232; BD), anti-I-COS (7E.17G9; 552146; BD), anti-CD200 (OX-90; 565543; BD), anti-PSGL-1 (2PH1; 555306; BD), anti-CD11a (2D7; 553121; BD), anti-CD180 (RP/14; 117706; BioLegend), anti-LAG3 (C9B7W; 552380; BD), anti-IL10Ra (2B11/CXCR4; 551966; BD), anti-CCR7 (4B12; 560682; BD), anti-RANK-L (IK22-5; 560295; BD), anti-CD309 (Avas12; 136403; BioLegend), anti-NKG2D (CX5; 558403; BD), anti-Thy1.2 (30-H12; 105312; BioLegend), anti-Thy1.1 (OX-7; 202504; BioLegend), anti-GATA3 (L50-823; 560074 and 560163; BD), anti-Foxp3 (MF23; 560408 and 560401; BD) and anti-Rorγt (Q31-378; 562607 and 562894; BD) were used to stain the samples.

For unbiased fluorescence-activated cell sorting (FACS) screening, CD4$^+$ T cells isolated from the lung were stained with antibodies against markers (Mouse Cell Surface Marker Screening Panel; BD) or corresponding isotype-matched antibodies. A FACS Verse or FACS Canto ll was used for the multi-parameter analysis, and data were analyzed using the FlowJo software program (Tree Star).

Intravenous staining of CD4$^+$ T cells localized in the vasculature of the lung. Intravenous staining of CD4$^+$ T cells was carried out as previously described[55]. For intravascular cell staining of CD4$^+$ cells, mice were intravenously injected with 0.5 µg anti-CD4 antibody (RM4-4; 116006 and 116004; BioLegend) diluted in 100 µl PBS, 3 min before sampling.

Depletion of Foxp3$^+$ T cells by intranasal administration of *Diphtheria* toxin. For the depletion of Foxp3$^+$ cells, Foxp3-DTR transgenic or wild-type mice were treated with the intranasal administration of 100 ng *Diphtheria* toxin (Sigma–Aldrich) in 30 µl PBS, 1 h before the administration of *Aspergillus* antigen during the last 3 weeks of antigen administration.

Flow cytometry for the analysis of cytokine production. CD4$^+$ T cells isolated from the lung were stimulated with phorbol 12-myristate 13-acetate (50 ng ml^{-1}) and ionomycin (500 ng ml^{-1}) for 4 h in the presence of monensin (2 µM). Anti-IL-4 (11B11; 554436 and 562915; BD), anti-IL-5 (TRFK5; 554396; BD; and 504304; BioLegend), anti-IL-13 (eBio13A; 12-7133-41 and 53-7133-82; eBioscience), anti-IL-17 (TC11-18H10.1; 559502 and 563354; BD; and 506910; BioLegend) and anti-IFNγ (XMG1.2; 554411 and 554412; BD; and 17-7311-81; eBioscience) were used for intracellular staining of mouse samples.

***t*-SNE analysis.** *t*-SNE analysis was performed using the FlowJo software program (version 10.2; FlowJo).

Quantitative real-time PCR. Total RNA isolation, complementary DNA synthesis and quantitative real-time PCR were described previously[56]. Primers and Roche Universal probes were purchased from Sigma–Aldrich and Roche, respectively. The gene expression was normalized with the β-actin messenger RNA signals.

RNA-Seq. RNA-Seq was carried out as previously described[57]. Total cellular RNA was extracted with TRIzol reagent (Invitrogen). For complementary DNA library construction, we used a SMARTer Stranded Total RNA-Seq Kit v2-Pico Input Mammalian (Clontech) according to the manufacturer's protocol. Sequencing of library fragments was performed on the HiSeq 1500 System. For the data analysis, read sequences (50 base pairs) were aligned to the mm10 mouse reference genome (University of California, Santa Cruz; December 2011) using Bowtie 2 (version 2.0.0) and TopHat (version 1.3.2). The fragments per kilobase of exon per million mapped reads for each gene were calculated using Cufflinks (version 2.0.2).

Analysis and graphic display of RNA-Seq data. A total of 9,085 genes for which the maximum fragments per kilobase of exon per million mapped reads value in all samples was ≥1.0 were subjected to further analyses. A principal component analysis was performed using R (https://www.r-project.org/). Clustering was performed using APCluster (an R Package for Affinity Propagation Clustering). The transcriptional signatures of CD44^{hi}CD69^{lo}, CD44^{hi}CD69^{hi}CD103^{lo} and CD44^{hi}CD69^{hi}CD103^{hi} CD4$^+$ T cells were defined with genes for which the expression was eightfold higher or fourfold lower than that in CD44^{lo}CD69^{lo} CD4$^+$ T cells.

For the visualization of the co-regulation network, the 500 genes in the CD44^{hi} CD4$^+$ T cell groups that showed the greatest variation compared with the naive (CD44^{lo}CD69^{lo}) CD4$^+$ T cell group were subjected to further analyses. The first-neighbor genes were determined using the following two criteria: (1) a correlation of >0.8; and (2) a ratio of norm of 0.8–1.25. The network graph of 483 genes was visualized using Cytoscape (http://www.cytoscape.org/).

The genes specifically upregulated in CD44^{hi}CD69^{lo}, CD44^{hi}CD69^{hi}CD103^{lo} or CD44^{hi}CD69^{hi}CD103^{hi} CD4$^+$ T cells were determined as fibrosis-related genes when they were included in the gene lists of the indicated Gene Ontology terms. The first-neighbor Gene Ontology terms were determined using the following criterion: a Simpson coefficient of ≥0.2. Node connections were determined based on the overlap of related to elemental gene products among the Gene Ontology terms. The network graph of 483 genes and Gene Ontology terms was visualized using Cytoscape.

ATAC-Seq. ATAC-Seq was carried out as previously described, with minor modification[58,59]. Some 50,000 cells were pelleted and washed with 50 µl 1× PBS, followed by treatment with 50 µl lysis buffer. The nuclei were re-suspended in a 40-µl transposition reaction with 2 µl Tn5 transposase (15027865 and 15027866; Illumina) to tag and fragmentize the accessible chromatin. The reaction was incubated at 37 °C with shaking at 300 r.p.m. for 30 min. The fragmentized DNA was purified using a QIAGEN MinElute kit and amplified with 11 or 12 PCR cycles, based on the amplification curve. The libraries were sequenced for 50 cycles (paired-end reads) on a HiSeq 1500.

Analysis of ATAC-Seq data. The ATAC-Seq data were mapped to the mouse genome build NCBI37/mm9 using the Bowtie (version 2.4.2.6; http://bowtie-bio.sourceforge.net/index.shtml) and HOMER tag directories, which were created by the HOMER platform[60] (makeTagDirectory). Reproducible ATAC peaks were annotated to the closest gene or transcriptional start site with proximity-based annotation using HOMER annotatePeaks.pl (mm9 genome build)[60]. BigWig files were generated from the aligned SAM or BED file formats using SAMtools[61], BEDTools[62] and the University of California, Santa Cruz genomeGoverageBed and bedGraphToBigWig, and normalized to 1 million reads. Only regions called in both replicates were used in the downstream analysis. Peak intensities ('tags' column) were normalized as tags per 10 million reads in the original library. A downstream analysis and heat map generation were performed. The Integrative Genomics Viewer software program (https://software.broadinstitute.org/software/igv/) was used for the visualization of BiGWig files. A motif enrichment analysis was performed with the findMotifsGenome.pl command in the HOMER package using a 200-base pair window.

Measurement of the collagen level in the lung tissue. Quantification of the collagen level of the left lung was performed using a Sircol collagen assay (Biocolor).

Airway hyper-responsiveness. The airway function was assessed by measuring the changes in lung resistance in response to increasing doses of inhaled methacholine, as described previously[53].

Parabiosis. Mice were anesthetized, and the corresponding lateral aspects were shaved. These aspects were then incised from the hip to behind the ear, and sutured together with a surgical needle (91–2124; Sansyo) and suture thread (DEBB0404; Akiyama-Seisakusyo).

FTY720 treatment. From 10 d to 1 d before the assay, 25 µg FTY720 (10006292; Cayman) dissolved in 200 µl saline was administered intraperitoneally to each mouse once a day.

Anti-CD103 antibody treatment. At 8, 6, 4 and 2 d before the assay, 100 µg InVivoMAb anti-mouse CD103 (M290; BE0026; Bio X Cell) was administered intraperitoneally to each mouse once a day.

Statistical analysis. Data were analyzed with the GraphPad Prism software program (version 6). Comparisons were performed using the Mann–Whitney *U*-test (two tailed), an unpaired *t*-test, one-way analysis of variance (ANOVA) with Tukey's multiple comparisons test, or two-way ANOVA with Bonferroni's multiple comparisons test. $P < 0.05$ was considered to indicate statistical significance.

Reporting Summary. Further information on research design is available in the Nature Research Reporting Summary linked to this article.

Data availability

The data that support the findings of this study are available from the corresponding author upon reasonable request. The RNA-Seq and ATAC-Seq data reported in this paper are available under Gene Expression Omnibus accession number GSE133399.

Code availability

The code that supports the findings of this study is available from the corresponding author upon reasonable request.

References

50. Higashiyama, R. et al. Negligible contribution of bone marrow-derived cells to collagen production during hepatic fibrogenesis in mice. *Gastroenterology* **137**, 1459–1466.e1 (2009).
51. Rubtsov, Y. P. et al. Regulatory T cell-derived interleukin-10 limits inflammation at environmental interfaces. *Immunity* **28**, 546–558 (2008).
52. Kerzerho, J. et al. Programmed cell death ligand 2 regulates T_H9 differentiation and induction of chronic airway hyperreactivity. *J. Allergy Clin. Immunol.* **131**, 1048–1057.e2 (2013).
53. Hirahara, K. et al. Repressor of GATA regulates T_H2-driven allergic airway inflammation and airway hyperresponsiveness. *J. Allergy Clin. Immunol.* **122**, 512–520.e11 (2008).
54. Shinoda, K. et al. Thy1$^+$IL-7$^+$ lymphatic endothelial cells in iBALT provide a survival niche for memory T-helper cells in allergic airway inflammation. *Proc. Natl Acad. Sci. USA* **113**, E2842–E2851 (2016).
55. Mato, N. et al. Memory-type ST2$^+$CD4$^+$ T cells participate in the steroid-resistant pathology of eosinophilic pneumonia. *Sci. Rep.* **7**, 6805 (2017).
56. Onodera, A. et al. Menin controls the memory T_H2 cell function by maintaining the epigenetic integrity of T_H2 cells. *J. Immunol.* **199**, 1153–1162 (2017).
57. Onodera, A. et al. Spatial interplay between polycomb and trithorax complexes controls transcriptional activity in T lymphocytes. *Mol. Cell Biol.* **35**, 3841–3853 (2015).
58. Buenrostro, J. D., Giresi, P. G., Zaba, L. C., Chang, H. Y. & Greenleaf, W. J. Transposition of native chromatin for fast and sensitive epigenomic profiling of open chromatin, DNA-binding proteins and nucleosome position. *Nat. Methods* **10**, 1213–1218 (2013).
59. Shih, H. Y. et al. Developmental acquisition of regulomes underlies innate lymphoid cell functionality. *Cell* **165**, 1120–1133 (2016).
60. Heinz, S. et al. Simple combinations of lineage-determining transcription factors prime *cis*-regulatory elements required for macrophage and B cell identities. *Mol. Cell* **38**, 576–589 (2010).
61. Li, H. et al. The Sequence Alignment/Map format and SAMtools. *Bioinformatics* **25**, 2078–2079 (2009).
62. Quinlan, A. R. & Hall, I. M. BEDTools: a flexible suite of utilities for comparing genomic features. *Bioinformatics* **26**, 841–842 (2010).

nature research

Corresponding author(s): Toshinori Nakayama

Last updated by author(s): Jul 25, 2019

Reporting Summary

Nature Research wishes to improve the reproducibility of the work that we publish. This form provides structure for consistency and transparency in reporting. For further information on Nature Research policies, see Authors & Referees and the Editorial Policy Checklist.

Statistics

For all statistical analyses, confirm that the following items are present in the figure legend, table legend, main text, or Methods section.

n/a	Confirmed	
☐	☒	The exact sample size (*n*) for each experimental group/condition, given as a discrete number and unit of measurement
☐	☒	A statement on whether measurements were taken from distinct samples or whether the same sample was measured repeatedly
☐	☒	The statistical test(s) used AND whether they are one- or two-sided *Only common tests should be described solely by name; describe more complex techniques in the Methods section.*
☒	☐	A description of all covariates tested
☐	☒	A description of any assumptions or corrections, such as tests of normality and adjustment for multiple comparisons
☐	☒	A full description of the statistical parameters including central tendency (e.g. means) or other basic estimates (e.g. regression coefficient) AND variation (e.g. standard deviation) or associated estimates of uncertainty (e.g. confidence intervals)
☐	☒	For null hypothesis testing, the test statistic (e.g. *F*, *t*, *r*) with confidence intervals, effect sizes, degrees of freedom and *P* value noted *Give P values as exact values whenever suitable.*
☒	☐	For Bayesian analysis, information on the choice of priors and Markov chain Monte Carlo settings
☒	☐	For hierarchical and complex designs, identification of the appropriate level for tests and full reporting of outcomes
☒	☐	Estimates of effect sizes (e.g. Cohen's *d*, Pearson's *r*), indicating how they were calculated

Our web collection on statistics for biologists contains articles on many of the points above.

Software and code

Policy information about availability of computer code

Data collection	A FACS Verse (BD), FACSCantoII (BD), and FACSAriaIII (BD) were used for flow cytometry data collection. ZEISS LSM710 and KEYENCE BZ-X710 were used for acquisition of microscopy data. ABI StepONEPlus was used for quantitative real-time PCR.
Data analysis	Flowjo10.5.3 or 10.2 was used for flow cytometry analysis. Prism v6 or v7.0d(GraphPad) was used for statistical analysis. illumina's bclfastq v2.19, bowtie2(v2.3.4.3 ,v2.0.0 or v2.4.2.6), Samtools v1.3, Bamtools v2.5.1, tophat(v2 or v1.3.2), Cufflinks(v2.2.0 or v2.0.2), MACS2 v2.1.2, deepTools v3.1, Homer v4.10 and R v3.6.0 were used for RNA-sequenceing and ATAC-sequenceing analysis. R v3.6.0, julia v1.1.1 and Cytoscape v3.7.1 were used for network analysis. ImageJ v1.8.0_172 was used for microscopic analysis.

For manuscripts utilizing custom algorithms or software that are central to the research but not yet described in published literature, software must be made available to editors/reviewers. We strongly encourage code deposition in a community repository (e.g. GitHub). See the Nature Research guidelines for submitting code & software for further information.

Data

Policy information about availability of data

All manuscripts must include a data availability statement. This statement should provide the following information, where applicable:

- Accession codes, unique identifiers, or web links for publicly available datasets
- A list of figures that have associated raw data
- A description of any restrictions on data availability

RNA-seq and ATAC-seq dataset were deposited in the Gene Expression Omnibus(GEO) with the accession number GSE133399. The remaining data that support the findings of this study are available from the corresponding authors upon request. Materials will be provided with material transfer agreements in place as appropriate.

Field-specific reporting

Please select the one below that is the best fit for your research. If you are not sure, read the appropriate sections before making your selection.

☒ Life sciences ☐ Behavioural & social sciences ☐ Ecological, evolutionary & environmental sciences

For a reference copy of the document with all sections, see nature.com/documents/nr-reporting-summary-flat.pdf

Life sciences study design

All studies must disclose on these points even when the disclosure is negative.

Sample size	Sample sizes of experiments were chosen based on our previous research and similar reports in the literature.
Data exclusions	No data were excluded from the analysis.
Replication	Biological replicates were used for the confirmation of the reproducibility of the study. All experiments were performed independently more than 2 times, and all results described in the study could be reproduced. When representative results were shown, the experimental results were reproduced independently with similar results. The reproducibility of bulk RNA-seq results were evaluated in supplementary figure 3a and 3b.All replicates in bulk RNA-seq and ATAC-seq experiments were collected from different cohorts of mice in separate experiments.
Randomization	Age- and sex-matched mice were used in experiments to control the covariates. Rorcfl/fl mice and Rorcfl/fl Foxp3-cre mice were littermates.
Blinding	Before the assay, one of our lab members, who was not going to join the assay, numbered the mice. The analyst performed the experiments with the notion about only the identification number of each mouse.

Reporting for specific materials, systems and methods

We require information from authors about some types of materials, experimental systems and methods used in many studies. Here, indicate whether each material, system or method listed is relevant to your study. If you are not sure if a list item applies to your research, read the appropriate section before selecting a response.

Materials & experimental systems

n/a	Involved in the study
☐	☒ Antibodies
☒	☐ Eukaryotic cell lines
☒	☐ Palaeontology
☐	☒ Animals and other organisms
☒	☐ Human research participants
☒	☐ Clinical data

Methods

n/a	Involved in the study
☒	☐ ChIP-seq
☐	☒ Flow cytometry
☒	☐ MRI-based neuroimaging

Antibodies

Antibodies used

Antibodies flowcytometry:
Anti-CD3e (145-2C11, 553061, BD, 1:100),
anti-CD4 (RM4-5, 552775, lot#5254740, BD, 1:200),
anti-CD8a(53-6.7, 100725, lot#B225983, BioLegend, 1:100),
anti-CD44 (IM7, 103020, BioLegend, 1:100),
anti-CD62L (MEL-14, 553150, lot#0000040523, 553152, 560514, BD, 1:100),
anti-TCRb (H57-597, 553174, BD, 1:100),
anti-CD69 (H1.2F3, 561932, 560689, BD, 1:100),
anti-CD103 (2E7, 121421, BioLegend and M290, 557494, 557495, lot#5107887, BD, 1:100),
anti-CD25 (PC61, 553866, 561048, BD, 1:100),
anti-CD122 (IL-2Rb; TM-Beta 1, 553362, 564762, BD, 1:100),
anti-CD127 (IL7Ra; SB/199, 552543, 564175, BD, 1:100),
anti-CD30L (RM153, 559232, lot#39584, BD, 1:100),
anti-I-COS (7E.17G9, 552146, BD, 1:100),
anti-CD200 (OX-90, 565543, BD, 1:100),
anti-PSGL-1 (2PH1, 555306, lot#3354852, BD, 1:100),
anti-CD11a (2D7, 553121, BD, 1:100),
anti-CD180 (RP/14, 117706, lot#B193126, BioLegend, 1:100),
anti-LAG3 (C9B7W, 552380, BD, 1:100),
anti-IL10Ra (2B11/CXCR4, 551966, BD, 1:100),
anti-CCR7 (4B12, 560682, lot#63528, BD, 1:100),
anti-RANK-L (IK22-5, 560295, BD, 1:100),

anti-CD309 (Avas12, 136403, BioLegend, 1:100),
anti-NKG2D (CX5, 558403, BD, 1:100),
anti-Thy1.2 (30-H12, 105312, BioLegend, 1:100),
anti-Thy1.1 (OX-7, 202504, BioLegend, 1:100),
anti-GATA3 (L50-823, 560074, lot#5309556, 560163, lot#4094756, BD, 1:5),
anti-Foxp3 (MF23, 560408, 560401, lot#7093878, BD, 1:5),
and anti-Rorgt (Q31-378, 562607, 562894, lot#4164538, lot#5198797, BD, 1:5),
anti-IL-4 (11B11, 554436, TONBO, 562915, BD, 1:200),
anti-IL-5 (TRFK5, 554396, lot#5079752, BD, 504304, lot#B220005, Biolegend, 1:50),
anti-IL-13 (eBio13A, 12-7133-41, lot#E02110-1633, 53-7133-82, lot#4318974, eBioscience, 1:50),
anti-IL-17 (TC11-18H10.1, 559502, 563354, BD, 506910, BioLegend, 1:100),
anti-IFNg (XMG1.2, 554411, lot#6078731, 554412, lot#4307883, BD, 17-7311-81, eBioscience, 1:200)

For unbiased-FACS screening, CD4+ T cells isolated from the lung were stained with antibodies against markers (Mouse Cell Surface Marker Screening Panel, BD) or corresponding isotype-matched antibodies adjusted in same concentration.
Isotype antibody Pacific Blue (RTK2071, 400419, lot#B185139, BioLegend),
Isotype antibody Brilliant Violet 421 (RTK2071, 400439, BioLegend)
Isotype antibody Brilliant Violet 510 (MOPC-21, 400172, lot#B248103, BioLegend)
Isotype antibody FITC (eBRG1, 11-4301-85, lot#E00562-1631, eBioscience),
Isotype antibody Alexa Fluor488 (RTK2758, 400525, lot#B228070, BioLegend),
Isotype antibody PE (RTK2071, 400408, lot#B237565, BioLegend),
Isotype antibody PE/Cy7 (RTK2758, 400522, lot#B269631, BioLegend)
Isotype antibody APC (eBRG1, 17-4301-82, eBioscience)
Isotype antibody Alexa Fluor647 (RTK2071, 400418, lot#B200197, BioLegend)

Histology and immunofluorescence:
anti-CD4 (RM4-5, 552775, lot#5254740, BD, 1:200),
anti-CD3e (2C11, 12-0031-82, eBioscience, 1:100),
anti-CD69 (AF2386, R&D, 1:100),
anti-Type I collagen (LB-1102, LSL-LB-1102, LSL, 1:1000)

Intravenous staining:
anti-CD4 antibody (clone, RM4-4, 116006, lot#B211830, 116004, BioLegend, 0.5ug/mouse)

Anti-CD103 antibody treatment:
InVivoMAb anti-mouse CD103 (M290, BE0026, Bio X Cell, lot#700018J3, 100ug/mouse)

Validation

All of the antibodies in this study are commercially available. All antibodies have been validated by the vendors on their official website, and previous studies from other groups and our laboratory.

Animals and other organisms

Policy information about studies involving animals; ARRIVE guidelines recommended for reporting animal research

Laboratory animals	BALB/c, BALB/c Foxn1nu, C57BL/6, Collagen 1a2-GFP transgenic (C57BL/6 background), CD4-Cre (C57BL/6 background), Thy1.1 (BALB/c background) females of 6-8 weeks were used. Foxp3-YFP-IRES-Cre (C57BL/6 background), Rorcfl/fl (C57BL/6 background), of 6-8 weeks were used. "Depletion of regulatory T cell" (DEREG) (BALB/c background) males and females of 6-8 weeks were used.
Wild animals	This study did not involve wild animals.
Field-collected samples	This study did not involve samples collected from the field.
Ethics oversight	The research proposals were reviewed by the ethics committee for animals at Chiba University.

Note that full information on the approval of the study protocol must also be provided in the manuscript.

Flow Cytometry

Plots

Confirm that:

☒ The axis labels state the marker and fluorochrome used (e.g. CD4-FITC).

☒ The axis scales are clearly visible. Include numbers along axes only for bottom left plot of group (a 'group' is an analysis of identical markers).

☒ All plots are contour plots with outliers or pseudocolor plots.

☒ A numerical value for number of cells or percentage (with statistics) is provided.

Methodology

Sample preparation	The isolation of CD4+ T cells from the lung: After euthanasia, mice were perfused with 5 ml of cold PBS solution through the left and right ventricle respectively. Lungs were dissociated in a C-tube (Miltenyi Biotec) in digestion buffer (RPMI 1640 supplemented with collagenase type III (200 U/mL; Worthington) and DNase I (200 ug/mL; Sigma-Aldrich)) using a GentleMACS tissue dissociator (Miltenyi Biotec). After 30 min at 37°C, samples were treated with final GentleMACS dissociation. Cell suspensions were passed through a 70-um cell strainer (Greiner Bio-One). Lung mononuclear cells were separated using by Percoll solution (GE Healthcare).
Instrument	A FACS Verse (BD) and a FACS Canto ll (BD) were used for multi-parameter analysis. Cell sorting was performed on Aria lll (BD).
Software	Data were analyzed with FlowJo software (Treestar, Ashland, Ore).
Cell population abundance	CD4+ T cell populations were sorted to >95% purity post sort, as determined by flow cytometry.
Gating strategy	We provided the representative gating strategy in the paper.

☒ Tick this box to confirm that a figure exemplifying the gating strategy is provided in the Supplementary Information.